

**ENGINEERED BARRIER SYSTEM PERFORMANCE
ASSESSMENT CODES (EBSPAC) PROGRESS REPORT
OCTOBER 1, 1993, THROUGH SEPTEMBER 25, 1994**

Prepared for

**Nuclear Regulatory Commission
Contract NRC-02-93-005**

Prepared by

**Center for Nuclear Waste Regulatory Analyses
San Antonio, Texas**

October 1994



**ENGINEERED BARRIER SYSTEM PERFORMANCE
ASSESSMENT CODES (EBSPAC) PROGRESS REPORT
OCTOBER 1, 1993, THROUGH SEPTEMBER 25, 1994**

Prepared for

**Nuclear Regulatory Commission
Contract NRC-02-93-005**

Prepared by

Peter C. Lichtner

**Center for Nuclear Waste Regulatory Analyses
San Antonio, Texas**

October 1994

PREVIOUS REPORTS IN SERIES

<u>Number</u>	<u>Name</u>	<u>Date Issued</u>
CNWRA 92-019	TWITCH—A Model for Transient Diffusion, Electromigration, and Chemical Reaction in One Dimension, Version 1	August 1992
CNWRA 92-020	MARIANA—A Simple Chemical Equilibrium Module, Version 1.0	August 1992
Letter Report	Selection and Evaluation of Models for Substantially Complete Containment Example Problem	September 1992
Letter Report	Preliminary Assessment of Pitting Corrosion Models	September 1992
CNWRA 93-021	Engineered Barrier System Performance Assessment Codes (EBSPAC) Progress Report—October 1, 1992, through September 25, 1993	October 1993

ABSTRACT

The progress in developing the Engineered Barrier System Performance Assessment Codes (EBSPAC) during FY94 is described in this report. The code CTOUGH was developed based on enhancements to the existing two-phase fluid-flow code, VTOUGH. Improvements included free-format input files, multiple output files for plotting results at user-specified times and for time-history plots, and decreased computation time and computer memory. In addition, an electromigration code, GEM (General Electrochemical Migration), was developed to replace TWITCH and MARIANA for describing crevice corrosion and other reactive-transport related problems. The code GEM was applied to oxidation of spent fuel in the form of uraninite under conditions appropriate to a tuffaceous host rock. Qualitative agreement was obtained with field observations of the paragenesis of mineral alteration products uranophane and soddyite at the Peña Blanca natural analogue site. However, it was found that because of a large positive volume change of reaction, the reaction products occupied a greater volume than the reactant uraninite resulting in a negative porosity.

CONTENTS

Section	Page
FIGURES	vii
TABLES	ix
ACKNOWLEDGMENTS	xi
QUALITY OF DATA	xi
EXECUTIVE SUMMARY	xiii
1 INTRODUCTION	1-1
1.1 REGULATORY REQUIREMENT	1-1
1.2 REPORT ORGANIZATION	1-1
2 NEAR-FIELD ENVIRONMENT MODEL	2-1
2.1 INTRODUCTION AND RATIONALE	2-1
2.2 MODIFICATIONS TO THE VTOUGH CODE	2-1
2.3 DESCRIPTION OF CTOUGH	2-2
2.3.1 Execution of CTOUGH	2-2
2.3.2 Execution of Conversion Program	2-3
3 ELECTROMIGRATION FORMALISM WITH HOMOGENEOUS AND HETEROGENEOUS CHEMICAL REACTIONS	3-1
3.1 INTRODUCTION AND RATIONALE	3-1
3.2 COMPARISON WITH TWITCH	3-1
3.3 CHEMICAL REACTIONS	3-2
3.3.1 Reversible Homogeneous Reactions	3-2
3.3.2 Irreversible Homogeneous Reactions	3-4
3.3.3 Heterogeneous Reactions	3-4
3.3.4 Electrochemical Corrosion Reactions	3-6
3.3.4.1 Electrochemical Kinetics at a Metal Surface	3-7
3.3.4.2 Gap Geometry	3-8
3.3.5 Ion-Exchange Reactions	3-9
3.3.6 Diffuse Double-Layer Model	3-11
3.4 MASS CONSERVATION EQUATIONS	3-13
3.4.1 Electrochemical Flux Density	3-14
3.4.2 Electroneutrality	3-16
3.4.3 Partial Differential Equations Representing Mass Conservation	3-16
3.4.3.1 Reduced Transport Equations	3-17
3.4.4 Initial and Boundary Conditions	3-18
3.5 SOLUTION CURRENT DENSITY	3-19
3.5.1 Electroneutrality	3-21
3.5.2 Equal Diffusivities and Mobilities	3-23
3.6 NUMERICAL SOLUTION ALGORITHM	3-24
4 MODEL BENCHMARKING	4-1
4.1 MINERAL PRECIPITATION/DISSOLUTION	4-1

CONTENTS (cont'd)

Section	Page
4.2 COMPARISON OF GEM WITH ANALYTICAL SOLUTIONS FOR STEADY-STATE COUNTER-DIFFUSION	4-2
4.3 ION-EXCHANGE REACTIONS	4-3
5 APPLICATIONS	5-1
5.1 ELECTROCHEMICAL PROCESSES	5-1
5.2 COMPARISON OF GEM WITH CREVICE DIFFUSION EXPERIMENTS	5-1
6 SPENT FUEL OXIDATION	6-1
7 STRESS CORROSION CRACKING MODELING	7-1
8 SUMMARY	8-1
9 REFERENCES	9-1
APPENDIX A—CTOUGH I/O MODIFICATIONS	
APPENDIX B—IMPLICIT FINITE DIFFERENCE EQUATIONS	

FIGURES

Figure		Page
4-1	Numerical results for conditions approximating local chemical equilibrium in the three-component system A-B-C for pure diffusive transport showing: (a) solute	4-2
4-2	Comparison of GEM (solid curves) with analytical solutions (dots) for cylindrical and spherical geometry	4-3
4-3	Flushing of Na^+ and K^+ by a CaCl_2 solution	4-4
5-1	Electrochemical migration of Na^+ and Cl^-	5-2
5-2	Theoretical calculations with GEM of the pH for diffusion into a crevice with species-dependent diffusion coefficients (curves) compared with experiment (symbols).	5-2
6-1	Theoretical calculations with GEM describing oxidation of uraninite in a tuffaceous host rock showing (a) volume fraction profiles, and (b) porosity for an elapsed	6-3
6-2	Theoretical calculations with GEM describing oxidation of uraninite in a tuffaceous host rock showing (a) Eh and pH, and (b) total uranium and iron aqueous	6-3

TABLES

Table		Page
3-1	Possible exchange reactions involving primary and secondary species	3-9
3-2	Diffusion coefficients for a selected set of species in an aqueous solution at 25 °C. Values taken from Oelkers and Helgeson (1988).	3-15
6-1	Volume fractions of the primary mineral assemblage	6-1
6-2	Compositions of the inlet and initial fluid. Molality units are used with the exception of pH.	6-2
6-3	Possible replacement reactions of uraninite and the corresponding volume change assuming uranium is conserved	6-6

ACKNOWLEDGMENTS

This report was prepared to document work performed by the Center for Nuclear Waste Regulatory Analyses (CNWRA) for the Nuclear Regulatory Commission (NRC) under Contract No. NRC-02-93-005. The activities reported here were performed on behalf of the NRC Office of Nuclear Material Safety and Safeguards, Division of Waste Management. The report is an independent product of the CNWRA and does not necessarily reflect the views or regulatory position of the NRC.

The author gratefully acknowledges the contribution of Gustavo A. Cragnolino as author of Section 7, the technical reviews of Narasi Sridhar and Ross Bagtzoglou, and the programmatic review of Patrick C. Mackin. Appreciation is due to Bonnie L. Garcia for her assistance in the preparation of this report.

QUALITY OF DATA

DATA: Sources of data are referenced in each chapter. The respective sources of these data should be consulted for determining their levels of quality assurance.

EXECUTIVE SUMMARY

This report presents progress in FY94 on computer code development within the Engineered Barrier System Performance Assessment Codes (EBSPAC) program in the Engineered Barrier System (EBS) Element of the Center for Nuclear Waste Regulatory Analyses (CNWRA). During this fiscal year, enhancements to the two-phase fluid flow code VTOUGH were made resulting in a new code referred to as CTOUGH. This code has a number of improvements in input/output and computational efficiency over the original version. In addition, the computer codes TWITCH and MARIANA, developed at the CNWRA by Dr. John Walton for describing crevice corrosion processes, were replaced with the code GEM (General Electrochemical Migration).

GEM provides an enhanced computing environment for reactive-transport calculations in one-dimensional systems, incorporating electrochemical effects, mineral precipitation/dissolution reactions, adsorption, and aqueous complexing reactions. The code reads thermodynamic input data directly from an equivalent form of the EQ3/6 database. The mass conservation equations solved by GEM apply to a minimal set of components, referred to as primary species. An implicit finite difference algorithm is employed to solve the transport equations.

The code GEM was benchmarked for precipitation/dissolution-type reactions based on an independent semi-analytical solution developed by Lichtner (1991). In addition, GEM was applied to nonreactive diffusive transport in a 10- μm -wide crevice and compared with experimental results. The agreement between experiment and theory was qualitative with the experiments requiring longer times to reach steady-state. Finally, GEM was applied to the problem of alteration of spent fuel under oxidizing conditions. Specifically, the calculations considered the diffusion of oxidizing water into a porous medium consisting of uraninite (UO_2) and pyrite, similar to the Peña Blanca natural analogue site. Two uranium-bearing alteration products, uranophane and soddyite, were formed in qualitative agreement with the paragenesis observed at the Peña Blanca natural analogue site. However, the alteration products occupied a much larger volume than the original reactants, producing a negative porosity in the calculation. This result may have significant implications for disposal of high-level radioactive waste (HLW) above the water table, as is currently being considered at Yucca Mountain, Nevada. In any event, it will be a very difficult task to model the alteration of spent fuel with any degree of certainty if the large positive volume change of reaction prevails.

In addition, a modeling strategy for evaluating stress corrosion cracking has been addressed in this report. In the future, it is expected that the electrochemical modeling of the corrosion-related processes will be integrated and enhanced by the GEM code development.

1 INTRODUCTION

Engineered Barrier System Performance Assessment Codes (EBSPAC) form a suite of auxiliary codes, models, and analyses that are used to understand and evaluate the performance of the various components of the engineered barrier system (EBS). The objectives of the EBSPAC development task are to (i) develop and evaluate credible compliance determination models for assessing the performance of EBS components and subsystems, and (ii) develop an understanding of the near-field wasteform performance issues. The detailed models and analyses developed within EBSPAC support more simplified models used in the Source Term Code (SOTEC) for Total System Performance Assessment calculations. In FY93, waste package environmental models were investigated within the EBSPAC program (Sridhar et al., 1993a). This report presents progress made in FY94 on computer code development

1.1 REGULATORY REQUIREMENT

The EBS Element addresses the subsystem performance requirements in 10 CFR 60.113 for containment and gradual release rate. To support the evaluation of these requirements, detailed modeling activities are carried out in the EBSPAC development program. This report presents the progress on computer code development within the EBSPAC program. During this fiscal year, enhancements to the two-phase fluid flow code VTOUGH were made, resulting in a new code referred to as CTOUGH. This code has a number of improvements in input/output (I/O) and computational efficiency over the original version. In addition, the computer codes TWITCH and MARIANA, developed at the Center for Nuclear Waste Regulatory Analyses (CNWRA) by J. Walton (Walton and Kalandros, 1992a,b) for describing crevice corrosion processes, were replaced with the code GEM (General Electrochemical Migration). The rationale for developing the code GEM was the need to enhance computation time, add a database capability, and add additional processes such as sorption reactions which are not included in TWITCH. This report provides a detailed account of the equations programmed into GEM with the exception of adsorption described by the electrical double layer. As such, the report will serve as the basis for further development of GEM in the future. GEM extends the functionality of TWITCH and MARIANA by providing access to the EQ3/6 database. Mass conservation equations are formulated in terms of a minimal set of primary species. A self-consistent calculation of the solution current density provides for accurate charge balance. Logarithms of the species concentrations are used as the independent variables to account for widely spatially varying species concentrations within a crevice. Finally GEM is based on a fully coupled, global-implicit finite difference algorithm to solve the mass transport equations.

1.2 REPORT ORGANIZATION

First, modifications and additions to VTOUGH, which resulted in a new code, CTOUGH, are discussed. The procedure for running CTOUGH is described, and the details for constructing the input file are given in Appendix A, along with a list of the output files produced for plotting results. Next, the theoretical basis for the electromigration code, GEM, is described. Following this, the numerical approach used to solve the governing equations using a fully implicit finite difference algorithm is discussed briefly. Details of the algorithm are presented in Appendix B. The GEM code is benchmarked against a semi-analytical solution for reactive transport in a porous medium for a three-component system involving mineral precipitation-dissolution reactions. The GEM code provides for two-dimensional (2D) and three-dimensional (3D) cylindrical and spherical symmetric geometries. The 2D and 3D geometry is tested using a simple analytical solution for steady-state nonreactive transport. The code GEM is applied to several examples consisting of electromigration in a $\text{NaCl-HNO}_3\text{-H}_2\text{O}$ solution, ion-exchange

reactions, and comparison with the results of nonreactive diffusion experiments in a crevice with cylindrical symmetry. Finally, the GEM code is applied to dissolution of spent fuel in the form of UO_2 with precipitation of alteration products uranophane and soddyite. Large positive volume changes of reaction are found to occur if the reactions are balanced on uranium, resulting in a negative porosity. The report concludes with a review of recent developments in stress corrosion cracking.

2 NEAR-FIELD ENVIRONMENT MODEL

2.1 INTRODUCTION AND RATIONALE

To support near-field modeling efforts, it was deemed necessary to upgrade the two-phase fluid flow code VTOUGH (Nitao, 1989) currently in use at the CNWRA. The current version of VTOUGH installed at the CNWRA was inefficient to use in several aspects and did not compute all the requisite quantities needed for evaluating the near-field performance of a high-level nuclear waste (HLW) repository emplaced above the water table in unsaturated porous media. These aspects include the evaporation rate and relative humidity. The VTOUGH input file was rigidly formatted making it cumbersome to alter without causing error. Output from the VTOUGH code was captured from a screen dump and processed with a post-processor. This resulted in a large output file with wasted disk space and inefficient monitoring of the progress of the execution of the code. To correct the deficiencies in the original code, a free-format input file was developed, and output files for plotting were written at user-specified times. More efficient solvers were added to the code, including an efficient direct solver which reduced the amount of computer memory required as well as the computational time.

2.2 MODIFICATIONS TO THE VTOUGH CODE

Specifically, modifications to the VTOUGH code included:

- I/O
 - Free-format input
 - Output plot files created at user-specified times
 - Time-history plot files
- Solvers
 - Nonsymmetric Preconditioned Conjugate Gradient (NSPCG) package
 - Nested factorization
 - D4 direct solver
- Evaporation Rate Computation
- Relative Humidity Computation

There are about 15 available preconditioners and about an equal number of accelerators available in the NSPCG package, giving 225 different combinations. Comparing the various solvers is still ongoing. The most successful solver to date is the D4 solver which increases CPU time by a factor of 2.5 or more and reduces storage by a factor of 3 or more. As a consequence, much larger systems can be computed than were previously possible without increasing workstation memory requirements.

2.3 DESCRIPTION OF CTOUGH

The code VTOUGH (Nitao, 1989) solves the two-phase mass and energy conservation equations in a partially saturated porous medium with components water and air. CTOUGH is based on the VTOUGH requirements and is modified to provide more user-friendly I/O and reduce computer computation time and memory. It was found that computation time could be reduced by at least a factor of 2.5 and memory by a factor of 3.5 or more, depending on the problem. This enables larger problems to be run with finer grids in two or three spatial dimensions.

The CTOUGH could be used in future work to analyze moisture redistribution in the near-field region of a HLW repository resulting from the thermal perturbation caused by emplacement of the waste. CTOUGH may also be combined with the electromigration code GEM to analyze salinity buildup around waste packages due to reflux of liquid and evaporation/condensation effects. Currently, CTOUGH is being used to analyze the release of ^{14}C from the repository by providing a spatial and temporal description of the temperature field, saturation, and liquid and gas fluxes resulting from emplacement of HLW.

This section provides a brief introduction to running the CTOUGH code and the input file conversion program that converts from the old formatted input file to the new free-format version. Modifications to the input file and structure of the output files for plotting are presented in Appendix A.

2.3.1 Execution of CTOUGH

The computer program CTOUGH is executed by invoking the following command on a UNIX machine in a shell window:

```
ctough data      (for an interactive run)
```

```
ctough data &   (for a batch or background run)
```

where `ctough` is the name of the CTOUGH executable module, and `'datai'` is the name of the input file. Note that all data file names must end with the character `'i'`, and should not exceed seven characters. The last character `'i'` of the data file name should not be specified on the command line as shown above.

If a data file name is not specified, the default dataset named `'toughi'` will be used. If the specified or default data file does not exist in the current directory, the run is terminated. The system will ask the user to re-specify the dataset name for an interactive job and terminate if running in batch mode.

The output files are identified by the dataset name prefix as discussed in Appendix A. Thus, a number of jobs may be concurrently submitted which will produce different output files corresponding to different dataset names.

2.3.2 Execution of Conversion Program

To enable easy conversion from existing input files using the original version of VTOUGH, a conversion program was constructed to facilitate converting to the free-format input file used by CTOUGH. To execute the conversion program the user types:

```
convrt < dataold > datai
```

where **convrt** is the executable of the conversion program, **dataold** is the input file corresponding to the old fixed format, and **datai** is the converted new file compatible with the free-format modified CTOUGH.

Currently, the CTOUGH code is in the development and evaluation stage. A user's manual is planned to be issued in FY96 and will be followed by inclusion of the code in the software configuration management process at the CNWRA.

3 ELECTROMIGRATION FORMALISM WITH HOMOGENEOUS AND HETEROGENEOUS CHEMICAL REACTIONS

3.1 INTRODUCTION AND RATIONALE

Modeling efforts directed toward understanding crevice corrosion at a fundamental level form a cornerstone of the EBSPAC program. To this end, a general formalism for incorporating both homogeneous and heterogeneous chemical reactions in a description of electrochemical reaction and migration was developed. The approach presented here takes into account formation of secondary reaction products at a corroding metal surface, including irreversible mineral precipitation/dissolution reactions and adsorption. Electrochemical effects may have several different origins (Newman, 1991). One possible contribution is diffusion of ionic species with differing diffusion coefficients. An electric field is established that acts on the charged species and influences their rate of migration in order to maintain electroneutrality of the aqueous solution. Another contribution is the electrochemical reaction of solids involving the transfer of electrons. Half-cell reactions are not balanced locally, in general, but may occur at spatially distinct locations resulting in the formation of an electric current in both the aqueous solution and solid phase matrix.

The general formulation presented below details the equations programmed into the revised code GEM which replaces TWITCH and MARIANA. The finite difference formulation of these equations appears in Appendix B.

3.2 COMPARISON WITH TWITCH

The code GEM replaces and generalizes the code TWITCH (Walton and Kalandros, 1992a) for describing crevice corrosion. Several advantages of GEM compared to TWITCH are:

- GEM incorporates thermodynamic data directly from an equivalent form of the EQ3/6 database (Wolery, 1983), whereas TWITCH requires the stoichiometry and standard state free energies of each reaction to be entered into the input file.
- GEM employs a self-consistent calculation of the solution current density that provides for accurate charge balance. By contrast, in TWITCH, the error in charge balance incurred during a calculation was redistributed over the aqueous species. The approach used in TWITCH could lead to inconsistencies in evaluating the results. The electrical balance *must* be maintained by the transport equations themselves and, therefore, can be used as a test of the numerical accuracy of the calculated result rather than forcing the result by altering the species concentrations in ways that may be inconsistent with the governing equations.
- By using the logarithms of the species concentrations as the independent variables, GEM can account for widely spatially varying concentration profiles of a species within a crevice. TWITCH did not always converge under such circumstances.
- The mass balance equations solved by GEM are formulated in terms of a minimal set of primary species. TWITCH uses separate transport equations for each species in solution.

- TWITCH uses an uncoupled approach for combining local equilibrium reactions with transport. A fully coupled, global-implicit finite difference algorithm is employed in GEM to solve the mass transport equations. This has a distinct advantage over an explicit approach in run time because of the increased time-step size allowed in the implicit method.

A number of other models have been developed describing electrochemical reactions coupled to transport in a crevice and open pit (Newman and Tobias, 1962; Sharland, 1987, 1992; Sharland et al., 1989; Macdonald and Urquidi-Macdonald, 1990a,b; Turnbull, 1993; Verbrugge et al., 1993a,b). However, none of these models appears to include as wide a range of processes as those incorporated into GEM.

3.3 CHEMICAL REACTIONS

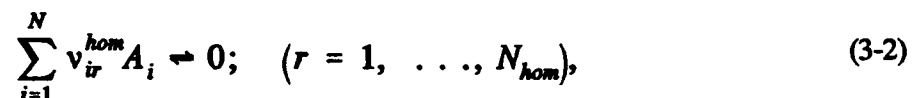
Reactions of potential importance involving the geochemistry of the near-field environment of an HLW repository are homogeneous complexing reactions within the aqueous phase, precipitation and dissolution of minerals, adsorption reactions, the formation of gaseous species, and possible electrochemical corrosion processes including dissolution of the spent fuel. Such reactions may be represented generally in the form



where v_{ir} denotes the stoichiometric reaction matrix and A_i denotes the symbol for the i^{th} species. To incorporate these reactions with flow and transport, it is advantageous to introduce a minimal set of primary species in terms of which all reactions can be expressed. This is done in the following sections for reversible and irreversible homogeneous reactions within the aqueous phase, heterogeneous reactions involving solids, and the aqueous solution and electrochemical reactions.

3.3.1 Reversible Homogeneous Reactions

Homogeneous reactions within the aqueous solution may be classified as reversible or irreversible depending on how rapidly the reaction takes place. For sufficiently fast reactions, local equilibrium can be assumed, thereby greatly simplifying the transport equations. For slow reactions, a kinetic rate law must be provided. For these irreversible reactions, it is important to distinguish between reactants and products that define the reaction mechanism. For reversible reactions, this is not the case, and it is arbitrary which species are referred to as reactants and which as products. With this in mind, the complete set of reversible and irreversible homogeneous reactions can be written in the general form



where v_{ir}^{hom} denotes the stoichiometric reaction matrix, and it is assumed that there are a total of N species participating in N_{hom} homogeneous reactions with

$$N_{hom} = N_{rev} + N_{irr}, \quad (3-3)$$

where N_{rev} denotes the number of reversible and N_{irr} the number of irreversible homogeneous reactions.

To simplify the resulting mass conservation equations, it is useful to express the homogeneous reactions in an alternative form (Lichtner, 1985). Rearranging the reactions, if necessary, so that the first N_{rev} reactions correspond to the reversible reactions and the remaining N_{irr} reactions correspond to the irreversible ones, the first N_{rev} reactions can be expressed as

$$\sum_{i=1}^{N_{rev}} \nu_{ir}^{hom} A_i \rightleftharpoons - \sum_{j=1}^{N-N_{rev}} \nu_{j+N_{rev}, r}^{hom} A_j + N_{rev}. \quad (3-4)$$

If it is also assumed that the N aqueous species are ordered in such a manner that the square matrix ν_{ir}^{hom} ($i, r = 1, \dots, N_{rev}$) appearing on the left-hand side is nonsingular, these reactions may be solved for the first N_{rev} species in terms of the remaining $N - N_{rev}$ species. These latter species are referred to as primary (or basis) species and denoted by B_j . In what follows, the subscript j is reserved for primary species. There are a total of $N - N_{rev} = N_{pri}$ such species. Multiplying through by the inverse matrix $(\nu^{hom})_{ri}^{-1}$ and renumbering the species, if necessary, yields the set of reactions

$$\sum_{j=1}^{N_{pri}} \tilde{\nu}_{ji} B_j \rightleftharpoons A_i; \quad (i = 1, \dots, N_{rev}), \quad (3-5)$$

where the matrix $\tilde{\nu}_{ji}$ is defined by

$$\tilde{\nu}_{ji} = - \sum_{r=1}^{N_{rev}} \nu_{jr}^{hom} (\nu^{hom})_{ri}^{-1}. \quad (3-6)$$

Each reaction is characterized by a different aqueous species A_i referred to as a secondary species.

For reversible reactions, mass action expressions exist relating the concentrations of the reacting species to the concentrations of the primary species. The concentration of the i^{th} secondary species is given in terms of the concentrations of the primary species by the relation

$$C_i = (\gamma_i)^{-1} K_i \prod_{j=1}^{N_{pri}} (\gamma_j C_j)^{\nu_{ji}}, \quad (3-7)$$

where K_i denotes the equilibrium constant, and γ_i denotes the activity coefficient of the subscripted species.

3.3.2 Irreversible Homogeneous Reactions

Irreversible homogeneous reactions within the aqueous phase are especially important for describing oxidation/reduction reactions. In natural waters, redox couples are generally not in thermodynamic equilibrium, and, hence, a redox potential cannot be defined. In such cases, it is imperative to describe such reactions using a kinetic rate law. Returning to the reactions (3-2), the remaining irreversible homogeneous reactions can be expressed in terms of the primary and secondary species according to



Replacing the secondary species by their equivalent represented by the left-hand side of the reaction (3-5) yields:

$$\sum_{j=1}^{N_{prt}} \tilde{\nu}_{jr} B_j \rightarrow 0, \quad (3-9)$$

where

$$\tilde{\nu}_{jr} = \nu_{jr} + \sum_i \tilde{\nu}_{ji} \nu_{ir}. \quad (3-10)$$

Therefore, the irreversible homogeneous reactions can be expressed solely in terms of the primary species. One possible expression for the reaction rate is in the form of an elementary reaction given by

$$I_r^{irr} = k_r^f \prod_{\tilde{\nu}_{jr} > 0} (\gamma_j C_j)^{\tilde{\nu}_{jr}} - k_r^b \prod_{\tilde{\nu}_{jr} < 0} (\gamma_j C_j)^{-\tilde{\nu}_{jr}}, \quad (3-11)$$

where $k_r^{f,b}$ denote the forward and backward rate constants.

3.3.3 Heterogeneous Reactions

In what follows, all mineral reactions are assumed to be irreversible, described by an overall reaction of the general form



These reactions do not necessarily represent the actual reaction mechanism that could involve several coupled reactions in parallel or series. They may be expressed in terms of the primary or basis species, B_j , by writing the reaction explicitly in terms of primary and secondary species as follows



Replacing the secondary species by their equivalent expression according to reactions (3-5), it follows that



which involves only the primary species $\{B_j\}$, where

$$\tilde{\nu}_{jm} = \nu_{jm} + \sum_{i=1}^{N_{rev}} \tilde{\nu}_{ji} \nu_{im}. \quad (3-15)$$

The form of the reaction rate is based on transition state theory (Lasaga, 1981). Precipitation or dissolution may occur depending on the sign of the affinity A_m of the reaction, defined by

$$A_m = -RT \ln K_m Q_m, \quad (3-16)$$

where K_m denotes the corresponding equilibrium constant, Q_m the ion activity product defined by

$$Q_m = \prod_j (\gamma_j C_j)^{\nu_{jm}}, \quad (3-17)$$

with R the gas constant and T the temperature. At equilibrium, the affinity and reaction rate vanish. The expression for the reaction rate must take into account the moving boundary nature of the transport-reaction problem. This can be accomplished with the form

$$I_m = -k_m s_m (1 - e^{-A_m/RT}), \quad \text{if } \phi_m > 0, \text{ or if } \phi_m = 0 \text{ and } A_m < 0, \quad (3-18)$$

or

$$I_m = 0, \quad \text{otherwise}, \quad (3-19)$$

where k_m denotes the kinetic rate constant, ϕ_m denotes the mineral volume fraction, and s_m denotes the mineral surface area participating in the reaction. Thus, the reaction rate vanishes if the aqueous solution is undersaturated with respect to the mineral in question, and the mineral is not present at the point of evaluation along the flow path. If the mineral is present, then either dissolution or precipitation occurs depending on the saturation state of the mineral. The rate has units of moles per unit time per unit volume of bulk porous medium and is taken as positive for reaction to the right and negative to the left. Thus, it represents an average rate taken over a representative elemental volume (REV). This form of the rate also includes overall oxidation/reduction reactions in which the electron does not occur explicitly.

The kinetic rate law given in Eq. (3-18) should really be referred to as a pseudokinetic rate law. Because it refers to the overall mineral precipitation/dissolution reaction, it generally does not describe the actual kinetic mechanism by which the mineral reacts. Nevertheless, it provides a useful form to describe departures from equilibrium. Close to equilibrium, the rate becomes proportional to the chemical affinity. With increasing rate constant k_m , the reaction rate approaches the local equilibrium result.

Likewise, reactions with a similar form hold for the gas species G_l :



where

$$\tilde{v}_{jl}^G = v_{jl} + \sum_{i=1}^{N_{rev}} \tilde{v}_{ji} v_{il}, \quad (3-21)$$

for the l^{th} gas species.

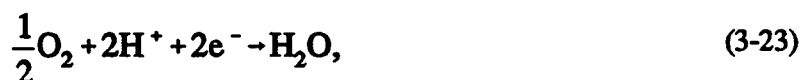
The stoichiometric reaction matrices \tilde{v}_{jl} , \tilde{v}_{jm} , and \tilde{v}_{jl}^G give the number of moles of the j^{th} primary species in one mole of the i^{th} aqueous complex, m^{th} mineral, and l^{th} gas, respectively. The corresponding rates of reaction, taken as positive for reaction to the right and negative to the left, are denoted by I_i , I_m , and I_l^G , respectively. The reaction rates have units of moles per unit of time per unit volume of bulk porous medium. Thus, they represent average rates taken over a REV.

3.3.4 Electrochemical Corrosion Reactions

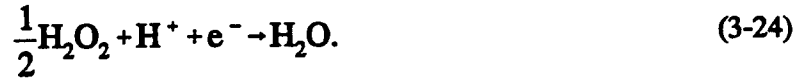
The electron, e^- , plays a special role in electrochemical processes. It is not included among the set of primary species because reactions within the aqueous phase can always be expressed as complete oxidation/reduction reactions and not as half reactions. In contrast, reactions at the metal surface are generally half reactions. The other half of the redox process may occur at a spatially separated reaction site. The electrochemical dissolution or corrosion of a metal, M , is assumed to have the form of the half reaction



where the metal ions M^{n+} are released into solution at the metal surface. The electrons, however, are conducted through the metal where they participate in reduction of oxidizing agents, such as O_2 , H_2O_2 , etc. For example, one possible reaction is the formation of water by reducing oxygen:



or hydrogen peroxide:



This reaction may occur at some distant site at the surface of the undisturbed metal away from the pit or crevice where the electrons are produced. A set of simultaneous corrosion reactions may be expressed generally in terms of primary species and the electron as



for the k^{th} metal M_k . The convention used here in writing corrosion reactions is in keeping with the general form given above in which the primary species occur on the left-hand side of the reaction. Because this reaction takes place at the surface of the corroding metal, its rate, denoted by I_k^{corr} , occurs as a source/sink term in the mass transport equations for the affected primary species. The corrosion rate is averaged over a REV in the crevice, expressed in units of moles per unit time per bulk volume of porous medium making up the crevice. In many cases, the electron is transported away from the site of the corrosion reaction through the metal and, therefore, does not affect directly the solution chemistry within the crevice. In this situation, half reactions involving the electron are not balanced locally. The number of electrons, n_k , participating in the k^{th} corrosion reaction is related to the valences of the primary species by charge balance

$$n_k = z_k - \sum_j z_j \nu_{jk}^{\text{corr}}. \quad (3-26)$$

3.3.4.1 Electrochemical Kinetics at a Metal Surface

For surface-controlled electrochemical reaction, the current density associated with the corroding metal can be expressed in the form of a Butler-Volmer type equation as

$$i_k = i_k^{\text{eq}} \left\{ \exp \left[\frac{\alpha_k n_k F}{RT} \eta_k \right] - \exp \left[- \frac{(1 - \alpha_k) n_k F}{RT} \eta_k \right] \right\}, \quad (3-27)$$

where i_k^{eq} denotes the equilibrium exchange current density and F is the Faraday constant. The first term represents the anodic and the second term the cathodic current density. The potential, η_k , refers to the overpotential defined as the difference between the actual potential and the equilibrium potential

$$\eta_k = E_{\text{corr}} - E_k^{\text{eq}}, \quad (3-28)$$

where E_{corr} is the corrosion potential established at the surface due to the superposition of all electrochemical reactions and where E_k^{eq} denotes the equilibrium potential for the electrochemical reaction (3-25) determined according to the Nernst equation

$$E_k^{eq} = E_k^0 + \frac{RT}{n_k F} \sum_j \nu_{jk}^{corr} \ln a_j, \quad (3-29)$$

where E_k^0 denotes the standard state potential. The parameter α_k can be determined from a Tafel plot relating the overpotential to the logarithm of the current density relative to the exchange current density:

$$\eta_k = \frac{RT \ln 10}{\alpha_k z_k F} \log \left[\frac{i_k}{i_k^{eq}} \right], \quad (3-30)$$

valid for

$$\frac{\alpha_k z_k F}{RT} \eta_k > 1, \quad (3-31)$$

or

$$\eta_k = -\frac{RT \ln 10}{(1 - \alpha_k) z_k F} \log \left[-\frac{i_k}{i_k^{eq}} \right], \quad (3-32)$$

valid for

$$-\frac{(1 - \alpha_k) z_k F}{RT} \eta_k > 1. \quad (3-33)$$

3.3.4.2 Gap Geometry

For a one-dimensional crevice between two identically corroding metals with gap width, l_g , the corrosion rate at the metal-solution interface must be averaged over the volume of the crevice. The surface-to-volume ratio is given by

$$\frac{\text{surface area}}{\text{solution volume}} = \frac{2A}{l_g A} = \frac{2}{l_g}, \quad (3-34)$$

where A denotes a unit area of the crevice surface. The factor two arises because there are two surfaces at the top and bottom of the crevice.

The volume averaged corrosion rate, I_k^{corr} , which appears in the transport equations is related to the electrochemical corrosion current by the expression

$$I_k^{corr} = -\frac{2}{Fn_k l_g} i_k \quad (3-35)$$

The total current density, i_e , at the metal-solution interface is related to the corrosion rates, I_k^{corr} , by the expression

$$\begin{aligned} i_e &= \sum_k i_k, \\ &= -F \frac{l_g}{2} \sum_k n_k I_k^{corr}. \end{aligned} \quad (3-36)$$

The current defined here refers to the local current in the crevice. It does not include the reduction current outside the crevice.

3.3.5 Ion-Exchange Reactions

Ion-exchange reactions taking place between the aqueous solution and solid phases include exchange between primary and secondary species. The different possibilities are shown in the accompanying table (Table 3-1). The exchange reactions may be expressed in the form



and



where solid exchange sites are denoted by the hypothetical species X^{α} . The valence of the l^{th} species is denoted by z_l . For adsorption of a species with valence z , X_z^{α} exchange sites are occupied. The respective exchange rates are denoted by $I_{j'}$, $I_{j'}$, and $I_{i'}$. They satisfy the anti-symmetry condition

$$I_{ji} = -I_{ij}, \quad (3-40)$$

Table 3-1. Possible exchange reactions involving primary and secondary species

Indices	Species types
j, j'	primary—primary
j, i	primary—secondary
i, i'	secondary—secondary

with similar relations for $I_{j'}$ and $I_{i'}$. For an aqueous complex, z_i is given by

$$z_i = \sum_j v_{ji} z_j. \quad (3-41)$$

The corresponding mass action equation is given by

$$K_{ij} = \left(\frac{a_j}{\bar{C}_j} \right)^{z_i} \left(\frac{\bar{C}_i}{a_i} \right)^{z_j}. \quad (3-42)$$

Conservation of exchange sites is expressed by

$$Q = \sum_j z_j \bar{C}_j = (1 - \phi) \rho Q_{CEC}, \quad (3-43)$$

where \bar{C}_j denotes the sorbed concentration of the j^{th} primary species, ρ refers to the density of the solid, and Q_{CEC} denotes the cation exchange capacity of the porous medium with the units moles sites/mass solid. These reactions conserve charge separately in the aqueous and solid phases. The exchange isotherm can be calculated from the mass action equation

$$\bar{C}_j = \frac{k_j a_j}{(k_i a_i)^{z_j/z_i}} \bar{C}_i^{z_j/z_i}, \quad (3-44)$$

where

$$k_{ij} = \frac{k_i^{z_j}}{k_j^{z_i}}, \quad (3-45)$$

for any $i \neq j$.

The dimensionless distribution coefficient, K_j^D , is defined as the ratio of solid to aqueous concentration by

$$K_j^D = \frac{\bar{C}_j}{C_j} = \frac{k_j \gamma_j}{(k_{j_0} a_{j_0})^{z_j/z_{j_0}}} \bar{C}_{j_0}^{-z_j/z_{j_0}}. \quad (3-46)$$

Alternatively define

$$\chi_j = \frac{z_j \bar{C}_j}{\sum_i z_i \bar{C}_i} = \frac{z_j \bar{C}_j}{Q}, \quad (3-47)$$

with the property that

$$\sum_j \chi_j = 1. \quad (3-48)$$

Then

$$K_{ji}' = \left(\frac{a_j}{\chi_j} \right)^{z_i} \left(\frac{\chi_i}{a_i} \right)^{z_j} = \frac{k_i'^{z_j}}{k_j'^{z_i}}, \quad (3-49)$$

where

$$k_i = \frac{Qk_i'}{z_i}. \quad (3-50)$$

The exchange isotherm \bar{C}_{j_0} is obtained from the equation

$$1 = \sum z_j \chi_j = z_{j_0} \bar{C}_{j_0} + \sum_{j \neq j_0} \frac{z_j k_j a_j}{(k_{j_0} a_{j_0})^{z_j/z_{j_0}}} \bar{C}_{j_0}^{-z_j/z_{j_0}}. \quad (3-51)$$

The derivative of the distribution coefficient can be obtained implicitly to give

$$\frac{\partial K_j^D}{\partial C_l} = - \frac{z_j K_j^D (K_j^D \delta_{jl} + K_l^D)}{\sum_i z_i \chi_i}. \quad (3-52)$$

Describing ion-exchange reactions in the presence of mineral precipitation and dissolution reactions can become very complicated because the surfaces on which exchange reactions are taking place may be dissolving or forming new layers.

3.3.6 Diffuse Double-Layer Model

The diffuse double-layer model for adsorption may be formulated generally in terms of the following set of surface complexation reactions



where $\bar{\chi}$ denotes the neutral oxide surface site, $\bar{\nu}_{ji}$ refers to the stoichiometric coefficients involving primary aqueous solute species A_j , and \bar{A}_i^{ad} represents the i^{th} adsorbed surface species. In what follows, an overscore is used to designate quantities which correspond to the surface of the oxide mineral.

Examples of these reactions for adsorption of a divalent cation M^{2+} on an oxide surface are expressed by



and



where $\equiv\text{XOH}_2^+$ and $\equiv\text{XO}^-$ represent surface hydroxyl groups describing protonation and deprotonation of the surface, $\equiv\text{XOH}$ represents the unoccupied surface sites, and $\equiv\text{XOM}^+$ represents adsorption of the cation M^{2+} .

The mass action equations corresponding to Eq. (3-53) have the general form

$$\bar{C}_i = \bar{K}_i C_{\bar{x}} \prod_{j=1}^N (\gamma_j C_j P^{z_j})^{\bar{v}_{ji}}, \quad (3-57)$$

$$= \bar{K}_i C_{\bar{x}} P^{\bar{z}_i} \prod_{j=1}^N (\gamma_j C_j)^{\bar{v}_{ji}},$$

where C_j denotes the bulk concentration of the j^{th} primary species, $C_{\bar{x}}$ the concentration of empty sites, and the factor P is given by the Boltzmann distribution

$$P = e^{-F\psi_0/RT}, \quad (3-58)$$

where ψ_0 denotes the electric double-layer potential evaluated at the surface. The latter expression is obtained noting that the valence associated with the i^{th} adsorbed species \bar{z}_i is related to the valences of the primary species by the equation

$$\bar{z}_i = \sum_j \bar{v}_{ji} z_j. \quad (3-59)$$

Conservation of sites is described by the equation

$$\begin{aligned}\bar{C}_s &= \bar{C}_x + \sum_i \bar{C}_i, \\ &= \bar{C}_x \left\{ 1 + \sum_i \bar{K}_i P^{\bar{z}_i} \prod_{j=1}^N (\gamma_j C_j)^{\bar{\nu}_{ji}} \right\}.\end{aligned}\tag{3-60}$$

From this relation and the mass action equation, Eq. (3-57), the sorption isotherms for the concentration of empty sites and adsorbed species are given by

$$\bar{C}_x = \frac{\bar{C}_s}{1 + \sum_i \bar{K}_i P^{\bar{z}_i} \prod_{j=1}^N (\gamma_j C_j)^{\bar{\nu}_{ji}}},\tag{3-61}$$

and

$$\bar{C}_i = \frac{\bar{C}_s \bar{K}_i P^{\bar{z}_i} \prod_{l=1}^N (\gamma_l C_l)^{\bar{\nu}_{li}}}{1 + \sum_{i'} \bar{K}_{i'} P^{\bar{z}_{i'}} \prod_{j=1}^N (\gamma_j C_j)^{\bar{\nu}_{ji'}}}.\tag{3-62}$$

The surface charge σ_0 is balanced by the total charge contained within the double-layer according to the expression

$$\begin{aligned}\sigma_0 &= F \sum_i \bar{z}_i \bar{C}_i, \\ &= \sqrt{2\epsilon DRT} \left[\sum_j C_j (e^{-z_j F \Psi_0 / RT} - 1) + \sum_i C_i (e^{-z_i F \Psi_0 / RT} - 1) \right].\end{aligned}\tag{3-63}$$

For a $z:z$ electrolyte, this equation simplifies to

$$\sigma = F \sum_i \bar{z}_i \bar{C}_i = \sqrt{2\epsilon DRT} \sinh \frac{F \Psi_0}{RT}.\tag{3-64}$$

A potential problem with the double-layer model of adsorption is that it does not conserve charge within the aqueous solution. Although the adsorption reaction given in Eq. (3-53), as do all chemical reactions, conserves charge, it does not conserve charge separately within the aqueous and solid phases. By contrast, the ion-exchange model does conserve charge separately in both phases. How important lack of charge conservation may be in reactive-transport calculations, and how the situation can be remedied if necessary, remain open questions.

3.4 MASS CONSERVATION EQUATIONS

The mathematical formulation of reactive transport in a multicomponent system is based on a macroscopic description of a porous medium. The porous medium is represented as a mathematical

continuum in which solid, gaseous, and aqueous phases coexist simultaneously at a single point in space. Field variables representing quantities such as temperature, pressure, solute, and mineral concentrations are averaged over a REV of the bulk porous medium. Chemical reactions involving solids, that take place microscopically at the surface of the solid, are represented as volume averaged rates by averaging the surface area over a REV. Mass conservation equations have the form of the continuity equation with a source/sink term on the right-hand side, accounting for the gain and loss of species due to chemical reactions. The mass conservation equation describing transport and reaction of the i^{th} solute species can be written in the general form

$$\frac{\partial \phi C_i}{\partial t} + \nabla \cdot J_i = R_i, \quad (3-65)$$

where ϕ denotes the porosity of the porous medium, C_i denotes the concentration, J_i denotes the species flux, and R_i represents a source-sink term describing the rate of production or depletion of the i^{th} species by chemical reactions.

3.4.1 Electrochemical Flux Density

For a sufficiently dilute aqueous solution, the flux density J_i for a dissolved species in a porous medium with porosity, ϕ , can be written in the form

$$J_i = -\tau \phi z_i \mu_i C_i F \nabla \Phi - \tau \phi D_i \nabla C_i + q C_i, \quad (3-66)$$

where the first term refers to electromigration, the second term to aqueous diffusion, and the last term to advective transport. Here, z_i , μ_i , and D_i denote the valence, mobility, and diffusivity of the i^{th} species, respectively, and τ refers to the tortuosity of the porous medium. The quantity Φ represents the electrical potential field, and q denotes the Darcy fluid velocity. The first term in the flux represents electromigration leading to a species-dependent flow velocity v_i^e defined by

$$v_i^e = -\tau \phi z_i \mu_i F \nabla \Phi, \quad (3-67)$$

which is proportional to the charge on the ion, the diffusivity, and the electric field gradient. The minus sign ensures that positively charged ions migrate in the direction of the electric field. A large electromigration velocity caused by a large potential gradient can lead to numerical instabilities in the finite difference schemes used to solve the mass transport equations as a consequence of the corresponding large Peclet number.

For more concentrated solutions, the flux must be written in terms of the chemical potential, μ_i , according to

$$J_i = -\tau \phi z_i \mu_i C_i F \nabla \Phi - \tau \phi u_i C_i \nabla \mu_i + q C_i, \quad (3-68)$$

where the chemical potential μ_i is defined by

$$\mu_i = \mu_i^0 + RT \ln a_i, \quad (3-69)$$

where μ_i^0 refers to the standard state chemical potential, and a_i denotes the activity of the i^{th} species defined by

$$a_i = \gamma_i C_i, \quad (3-70)$$

where γ_i denotes the activity coefficient. Noting that according to the Nernst-Einstein relation

$$D_i = RTu_i, \quad (3-71)$$

the solute flux can be expressed in the more concise form

$$J_i = -\tau\phi \frac{D_i C_i}{RT} \nabla(z_i F \Phi + \mu_i) + q C_i. \quad (3-72)$$

Substituting for the chemical potential from Eq. (3-68) and making use of the relation between activity and concentration yields the expression

$$J_i = -\tau\phi z_i u_i C_i F \nabla \Phi - \tau\phi D_i (\nabla C_i + C_i \nabla \ln \gamma_i) + q C_i, \quad (3-73)$$

This form of the flux is used in what follows. Values for diffusion coefficients of solute species in an aqueous solution are listed in Table 3-2.

Table 3-2. Diffusion coefficients for a selected set of species in an aqueous solution at 25 °C. Values taken from Oelkers and Helgeson (1988).

Species	Diffusion Constant $\text{cm}^2\text{s}^{-1} \times 10^5$	Species	Diffusion Constant $\text{cm}^2\text{s}^{-1} \times 10^5$	Species	Diffusion Constant $\text{cm}^2\text{s}^{-1} \times 10^5$
Ca^{2+}	0.9	OH^-	5.5	H^+	9.6
Cu^{2+}	0.8	F^-	2.1	K^+	1.8
Ni^{2+}	0.8	Cl^-	2.1	Na^+	1.4
Sr^{2+}	0.9	I^-	2.0	Cs^+	2.1
Zn^{2+}	0.8	NO_3^-	2.0	Cu^+	1.2

3.4.2 Electroneutrality

To complete the set of equations, one more equation is required to determine the electric potential Φ . The additional equation is provided by the requirement of electroneutrality within the aqueous solution implying that the total charge at any given point and time must vanish

$$\sum_i z_i C_i = 0, \quad (3-74)$$

where the sum is over all charged species including primary and reversibly and irreversibly reacting aqueous species. In the absence of electrochemical processes, this condition is ensured automatically by the transport equations, provided that the initial and boundary conditions are electrically balanced and an additional equation is not required. However, this is not the case when electrochemical processes are present.

3.4.3 Partial Differential Equations Representing Mass Conservation

Partial differential equations representing mass conservation incorporating the above reactions take the following form for primary species,

$$\begin{aligned} \frac{\partial}{\partial t}(\phi C_j) + \nabla \cdot J_j = & - \sum_m \bar{v}_{jm} I_m - \sum_i \bar{v}_{ji} I_i^{rev} \\ & - \sum_r v_{jr} I_r^{irr} - \sum_k v_{jk}^{corr} I_k^{corr} - \sum_l z_l I_{jl}^{ad}, \end{aligned} \quad (3-75)$$

for secondary species,

$$\frac{\partial}{\partial t}(\phi C_i) + \nabla \cdot J_i = I_i^{rev}, \quad (3-76)$$

for minerals,

$$\frac{\partial}{\partial t} \phi_m = \bar{V}_m I_m, \quad (3-77)$$

and for adsorption

$$\frac{\partial \bar{C}_l}{\partial t} = \sum_j z_j I_{jl}^{ad}, \quad (3-78)$$

with sorbed concentration \bar{C}_l . All rates are volume averaged over a REV regardless of whether they occur at the solid-solution interface or occur homogeneously within the aqueous solution.

3.4.3.1 Reduced Transport Equations

Eliminating the rates for reversible reactions involving aqueous secondary species and adsorbed species from the primary species transport equations yields

$$\frac{\partial}{\partial t} \left(\phi \Psi_j + \sum_i \bar{C}_i \right) + \nabla \cdot \mathbf{\Omega}_j = - \sum_m \tilde{v}_{jm} I_m - \sum_r v_{jr} I_r^{irr} - \sum_k v_{jk}^{corr} I_k^{corr}, \quad (3-79)$$

where

$$\Psi_j = C_j + \sum_i \tilde{v}_{ji} C_i, \quad (3-80)$$

and

$$\mathbf{\Omega}_j = J_j + \sum_i \tilde{v}_{ji} J_i. \quad (3-81)$$

In the presence of electrochemical processes, the expression for the generalized flux in the aqueous phase can be written in the form

$$\mathbf{\Omega}_j = -\tau \phi \Psi_j^\epsilon F \frac{\nabla \Phi}{RT} - \tau \phi (\Gamma_j^D + \Gamma_j^Y) + q \Psi_j, \quad (3-82)$$

obtained by inserting the expression for the flux defined in Eq. (3-72) into equation Eq. (3-80), where

$$\Gamma_j^D = D_j \nabla C_j + \sum_i v_{ji} D_i \nabla C_i, \quad (3-83)$$

$$\Gamma_j^Y = D_j C_j \nabla \ln \gamma_j + \sum_i v_{ji} D_i C_i \nabla \ln \gamma_i, \quad (3-84)$$

and where

$$\Psi_j^\epsilon = z_j D_j C_j + \sum_i v_{ji} z_i D_i C_i. \quad (3-85)$$

This form for the flux assumes that the diffusion coefficients are constants.

In the absence of electrochemical effects and assuming that the diffusion coefficients D_i are the same for all species for sufficiently dilute solutions, the generalized flux term $\mathbf{\Omega}_j$ reduces to the expression

$$\Omega_j = (-\tau\phi D\nabla + q)\Psi_j. \quad (3-86)$$

in which the flux is expressed entirely in terms of the generalized concentration Ψ_j . However, in the general case, this simplification is not possible.

Defining the quantity κ according to the expression

$$\begin{aligned} \kappa &= \tau\phi F^2 \left(\sum_j z_j^2 u_j C_j + \sum_i z_i^2 u_i C_i \right), \\ &= \frac{\tau\phi F^2}{RT} \sum_j z_j \Psi_j^e, \end{aligned} \quad (3-87)$$

the gradient in the electric potential can be expressed in terms of the current density according to

$$\begin{aligned} \nabla\Phi &= -\frac{1}{\kappa} i - \frac{\tau\phi F}{\kappa} \sum_j z_j \left(D_j \nabla C_j + \sum_i v_{ji} D_i \nabla C_i \right), \\ &= -\frac{1}{\kappa} i - \frac{\tau\phi F}{\kappa} \sum_j z_j \Gamma_j^D, \end{aligned} \quad (3-88)$$

where the latter expression holds for constant diffusivities. From this equation if the current density is a known function of the species concentrations, the gradient in the potential can be calculated.

Porosity and mineral volume fractions are related by an equation of the form

$$\phi = 1 - \sum_m \phi_m. \quad (3-89)$$

However, this expression is not completely general because of the difference in connected and total porosity. By relating the permeability and tortuosity to porosity through various phenomenological relations, it is possible to couple changes in porosity to the flow field.

3.4.4 Initial and Boundary Conditions

The mass transport equations are subject to the following initial and boundary conditions

$$C_j(0, t) = C_j^0, \quad (3-90)$$

$$C_j(x, 0) = C_j^\infty, \quad (3-91)$$

and

$$\frac{\partial C_j}{\partial x}(L, t) = 0, \quad (3-92)$$

for aqueous species. In addition the initial solid composition must be specified,

$$\phi_m(x, 0) = \phi_m^{\infty}, \quad (3-93)$$

and

$$\bar{C}_i^{\alpha}(x, 0) = \bar{C}_i^{\alpha 0}, \quad (3-94)$$

for primary species and a similar relation for secondary species

$$\bar{C}_i^{\alpha}(x, 0) = \bar{C}_i^{\alpha 0}. \quad (3-95)$$

3.5 SOLUTION CURRENT DENSITY

In general, the solution current density corresponding to the j^{th} primary species i_j is defined by

$$i_j = Fz_j\Omega_j. \quad (3-96)$$

The total current density in solution is given by the sum

$$i = \sum_j i_j, \quad (3-97)$$

over primary species. Substituting for the flux, the total current density can be expressed as

$$i = -\tau\phi F^2 \frac{\nabla\Phi}{RT} \sum_j z_j \Psi_j^{\epsilon} - \tau\phi F \sum_j z_j (\Gamma_j^D + \Gamma_j^Y). \quad (3-98)$$

Note that by the electroneutrality condition, the advective term vanishes. It follows that the gradient in the electric potential Φ , or electric field, can be expressed as

$$\nabla\Phi = -RT \frac{i + \tau\phi F \sum_j z_j (\Gamma_j^D + \Gamma_j^Y)}{\tau\phi F^2 \sum_i z_i \Psi_i^{\epsilon}}. \quad (3-99)$$

Separating the potential into current-independent Φ_0 and -dependent $\delta\Phi$ parts, it follows that

$$\nabla\Phi = \nabla\Phi_0 + \nabla\delta\Phi, \quad (3-100)$$

where $\nabla\Phi_0$ is defined by the equation

$$\nabla\Phi_0 = -\frac{\tau\phi F}{\kappa} \sum_j z_j (\Gamma_j^D + \Gamma_j^Y), \quad (3-101)$$

and $\nabla\delta\Phi$ by

$$\nabla\delta\Phi = -\frac{1}{\kappa} i. \quad (3-102)$$

Substituting for the gradient of the electric potential in the general form of the solute flux yields the following expression for the diffusive flux:

$$\begin{aligned} \Omega_j &= \frac{\Psi_j^\epsilon}{F \sum_l z_l \Psi_l^\epsilon} i + \tau\phi \Psi_j^\epsilon \frac{\sum_l z_l (\Gamma_l^D + \Gamma_l^Y)}{\sum_{l'} z_{l'} \Psi_{l'}^\epsilon} - \tau\phi (\Gamma_j^D + \Gamma_j^Y) + q\Psi_j, \\ &= \frac{\Psi_j^\epsilon}{F \sum_l z_l \Psi_l^\epsilon} i + \tau\phi \sum_l \left[\frac{\Psi_j^\epsilon z_l}{\sum_{l'} z_{l'} \Psi_{l'}^\epsilon} - \delta_{jl} \right] (\Gamma_l^D + \Gamma_l^Y) + q\Psi_j. \end{aligned} \quad (3-103)$$

In this form, the electric current appears rather than the electric potential. This expression can be recast in matrix form as

$$\Omega_j = \frac{1}{F} \omega_j i - \tau\phi \sum_l \beta_{jl} (\Gamma_l^D + \Gamma_l^Y) + q\Psi_j, \quad (3-104)$$

where the matrix β_{jl} is defined by

$$\beta_{jl} = \delta_{jl} - \omega_j z_l, \quad (3-105)$$

with

$$\omega_j = \frac{\Psi_j^\epsilon}{\sum_l z_l \Psi_l^\epsilon}. \quad (3-106)$$

The total flux can be expressed as

$$\Omega_j = \Omega_j^0 + \Omega_j^\Gamma + \Omega_j^\epsilon, \quad (3-107)$$

where

$$\mathbf{\Omega}_j^0 = -\tau\phi(\Gamma_j^D + \Gamma_j^r) + q\Psi_j, \quad (3-108)$$

$$\mathbf{\Omega}_j^r = \tau\phi\Gamma_j\sum_l z_l(\Gamma_l^D + \Gamma_l^r), \quad (3-109)$$

and

$$\mathbf{\Omega}_j^e = \frac{1}{F}\omega_j j. \quad (3-110)$$

The terms $\mathbf{\Omega}_j^e$ and $\mathbf{\Omega}_j^r$ incorporate the effects of the electric potential in maintaining charge balance.

The matrix β_{jl} is a projection operator, that is, it satisfies the relation

$$\sum_l \beta_{jl}\beta_{lk} = \beta_{jk}, \quad (3-111)$$

or in matrix notation:

$$\beta^2 = \beta. \quad (3-112)$$

Furthermore, it follows that

$$\sum_j z_j \beta_{jk} = 0, \quad (3-113)$$

which is a consequence of the relation

$$\sum_j z_j \omega_j = 1, \quad (3-114)$$

according to the definition of Γ_j .

3.5.1 Electroneutrality

The requirement of electroneutrality within the aqueous solution implies that

$$\sum_l z_l C_l = 0, \quad (3-115)$$

where the sum ranges over all charged species in the aqueous solution including both primary and secondary species. In terms of the generalized concentration, Ψ_j , the electroneutrality condition becomes

$$\sum_j z_j \Psi_j = 0. \quad (3-116)$$

If the initial and boundary conditions satisfy the condition of electroneutrality, the solution itself remains electrically neutral as it evolves in time. This can be seen as follows: multiplying the mass transport equations by z_j and summing over all primary species yields the equation

$$\begin{aligned} \frac{\partial}{\partial t} \left(\sum_j z_j \Psi_j \right) + \nabla \cdot \sum_j z_j \mathbf{\Omega}_j &= - \sum_{jm} z_j v_{jm} I_m - \sum_{jk} z_j v_{jk}^{corr} I_k^{corr}, \\ &= - \sum_k n_k I_k^{corr}, \end{aligned} \quad (3-117)$$

with all other terms on the right-hand side being equal to zero by conservation of charge of chemical reactions. The sum over the fluxes reduces to

$$\begin{aligned} \sum_j z_j \mathbf{\Omega}_j &= \sum_j z_j \mathbf{\Omega}_j^0 + \sum_j z_j \mathbf{\Omega}_j^{\Gamma} + \sum_j z_j \mathbf{\Omega}_j^e, \\ &= \frac{1}{F} \mathbf{i}, \end{aligned} \quad (3-118)$$

with the first two terms identically summing to zero:

$$\sum_j z_j [\mathbf{\Omega}_j^0 + \mathbf{\Omega}_j^{\Gamma}] = 0. \quad (3-119)$$

Written in terms of current densities, Eq. (3-117) becomes

$$\frac{\partial}{\partial t} \left(F \sum_j z_j \Psi_j \right) + \nabla \cdot \mathbf{i} = I_e, \quad (3-120)$$

with I_e the volume averaged electrochemical current density at the solution-metal interface given by

$$I_e = -F \sum_k n_k I_k^{corr} = \frac{2}{l_g} \sum_k i_k = \frac{2}{l_g} i_e. \quad (3-121)$$

If Eq. (3-115) is to hold identically, the divergence of the current density in solution must be equal to the current produced at the solution-metal interface, or in symbols

$$\nabla \cdot \mathbf{i} = I_e, \quad (3-122)$$

according to Eq. (3-119). Integrating over the crevice or pit volume leads to the integral form of the current densities:

$$\int_V \nabla \cdot i dV = \int_{\partial V} i \cdot d\sigma = \int_V i_e dV, \quad (3-123)$$

where ∂V denotes the metal surface bounding the volume of integration, V , corresponding to the pit or crevice. Because redox half reactions associated with electrochemical processes may be separated spatially, the electric current need not vanish locally. For a 1D system, these relations become

$$\frac{\partial i}{\partial x} = I_e, \quad (3-124)$$

and

$$\begin{aligned} i(x) &= \int_{x_0}^x I_e(x') dx', \\ &= -F \sum_k n_k \int_{x_0}^x I_k^{corr}(x') dx'. \end{aligned} \quad (3-125)$$

For constant rate I_k^0 , it follows that the current density varies linearly with x along the crevice:

$$i(x) = (x - x_0) \sum_k I_k^0, \quad (x_0 \leq x \leq L). \quad (3-126)$$

3.5.2 Equal Diffusivities and Mobilities

For equal diffusion coefficients,

$$D_i = D, \quad u_i = u, \quad (3-127)$$

it follows that

$$D_j \nabla C_j + \sum_i v_{ji} D_i \nabla C_i = D \nabla \Psi_j, \quad (3-128)$$

and the diffusivity term contributing to the current density i also vanishes. In this case,

$$i = -\tau \phi F^2 \frac{\nabla \Phi}{RT} \sum_j z_j \Psi_j^\epsilon = -\kappa \nabla \Phi, \quad (3-129)$$

and

$$\Psi_j^\epsilon = D \left(z_j C_j + \sum_i v_{ji} z_i C_i \right), \quad (3-130)$$

which does not, in general, vanish. Furthermore,

$$\begin{aligned}
 \sum_j z_j \Psi_j^\epsilon &= D(\sum z_j^2 C_j + \sum v_{ji} z_j z_i C_i), \\
 &= D(\sum z_j^2 C_j + \sum z_i^2 C_i), \\
 &= 2DI,
 \end{aligned}
 \tag{3-131}$$

where I denotes the ionic strength of the aqueous solution defined by

$$I = \frac{1}{2}(\sum z_j^2 C_j + \sum z_i^2 C_i).
 \tag{3-132}$$

In this case, the current density simplifies to

$$i = -2\tau\phi uIF^2\nabla\Phi.
 \tag{3-133}$$

3.6 NUMERICAL SOLUTION ALGORITHM

The numerical solution algorithm used in the GEM code is an implicit finite difference method using Newton-Raphson iteration to solve the nonlinear finite difference equations (see Appendix B). The implicit approach has a distinct advantage over the explicit method for small crevices. This is because the time-step size, Δt , in the explicit method is severely limited by stability considerations to a maximum value that depends on the diffusion coefficient and grid spacing by the relation

$$\Delta t \leq \frac{\Delta x^2}{2D}.
 \tag{3-134}$$

Therefore, for a given diffusion coefficient D , the smaller the grid size, the smaller the allowable time step. For example, for $D_{H^+} = 9.6 \times 10^{-5} \text{ cm}^2 \text{ s}^{-1}$, and for a 1-cm-long crevice with 100 node points each of width $\Delta x = 0.01 \text{ cm}$, the maximum time step is $\Delta t \sim 0.5$ seconds. Such a small time step could result in a real time simulation of a crevice experiment! By contrast, the fully backward implicit finite difference method is unconditionally stable and places no restriction on the time-step size.

4 MODEL BENCHMARKING

Special consideration must be given to evaluating computer codes designed to model flow and transport processes involving geologic time spans. There are two distinct criteria which must be kept in mind. One is whether the model in question can accurately represent the actual physical and chemical processes for which it was designed. And second, a somewhat easier problem, whether the code is solving the equations it was intended to solve. This latter aspect is dealt with here. As applies to long time spans, such as encountered in modeling the behavior of a nuclear waste repository, the question is to what extent can the modeler be assured that the code is delivering a sufficiently accurate approximation to the governing equations. Or has the solution been corrupted by round-off errors, for example, as a result of the many time steps involved to reach the desired simulation time. Fortunately, this question can be answered definitively for certain scalable systems (Lichtner, 1993), in spite of their highly nonlinear nature. In fact, for these systems it is easier to obtain the asymptotic solution to the transport equations than the earlier time behavior which generally requires solving a system of nonlinear partial differential equations. It is possible to demonstrate that the asymptotic solution is given by a set of algebraic equations which can be solved without the introduction of round-off error. This algebraic solution can then be used to determine the accuracy of the numerical method used to solve the corresponding partial differential equations. The algebraic solution results from pure advective transport under conditions of local chemical equilibrium. For diffusive transport, it is also necessary to solve an ordinary differential equation to determine the asymptotic state because of internal reaction within mineral alteration zones. This approach is used in the next section to test GEM in modeling precipitation/dissolution reactions over long time spans.

4.1 MINERAL PRECIPITATION/DISSOLUTION

Code validation for mineral precipitation/dissolution reactions was accomplished by comparing results with the semi-analytical solution based on the quasi-stationary state approximation obtained by Lichtner (1991), for the three-component system A-B-C. Two minerals $AB_{(s)}$ and $AC_{(s)}$ with molar volumes 74.69 and 36.934 $cm^3 mole^{-1}$, and $\log K's$ -4.44 and -5.29. These values correspond to gypsum and calcite, respectively, with the species A, B, and C analogous to Ca^{2+} , SO_4^{2-} , and CO_3^{2-} , respectively. A porous medium with porosity 10 percent initially containing the single solid $AB_{(s)}$ with a volume fraction of $\phi_{AB}^0 = 0.5$ is assumed in the calculation. The remaining portion of the porous medium is considered to be inert. An initial fluid in equilibrium with mineral $AB_{(s)}$ with solute concentrations $C_A^* = C_B^* = 6.0256 \times 10^{-3}$, and $C_C^* = 10^{-8}$ moles liter $^{-1}$, respectively, is assumed. Solute species A, B, and C with concentrations of $C_A^0 = 10^{-3}$, $C_B^0 = 10^{-8}$, $C_C^0 = 2 \times 10^{-3}$ moles liter $^{-1}$, respectively, are assumed to diffuse into the porous column with a diffusion coefficient of 10^{-5} $cm^2 s^{-1}$. The inlet solution is undersaturated with respect to mineral $AB_{(s)}$ which dissolves and is replaced by mineral $AC_{(s)}$. An effective kinetic rate constant for both minerals is used in the calculation with a value of 10^{-7} mole $cm^{-3} s^{-1}$.

The results of the calculation for an elapsed time of 100 years are shown in Figure 4-1. Profiles for the solute concentration, mineral volume fraction of secondary mineral $AC_{(s)}$, and reaction rates for

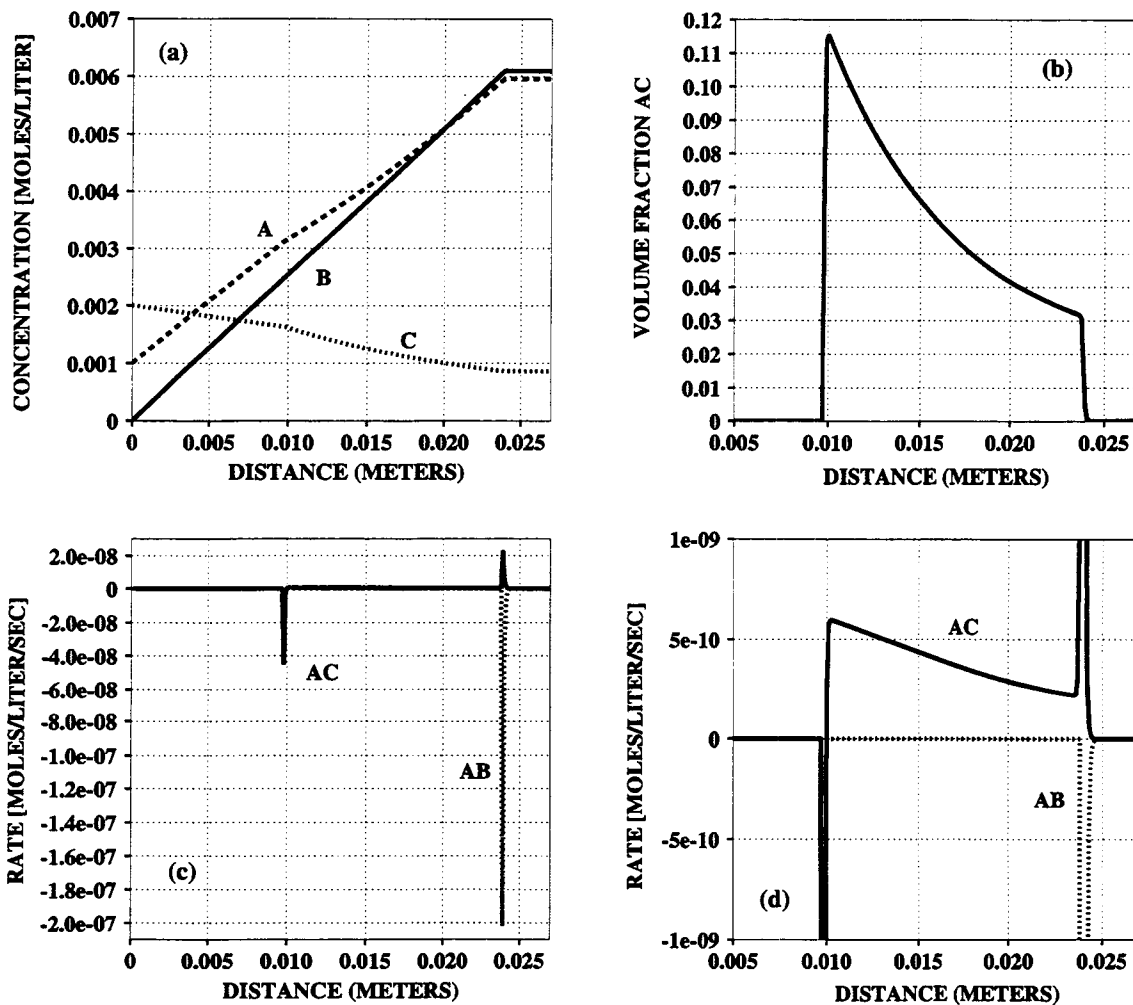


Figure 4-1. Numerical results for conditions approximating local chemical equilibrium in the three-component system A-B-C for pure diffusive transport showing: (a) solute concentration; (b) volume fraction of mineral AC; (c) and (d) reaction rates of minerals AB and AC plotted as a function of distance for an elapsed time of 100 years

both minerals are given, including a detail of the reaction rates in the vicinity of mineral $AC_{(s)}$. Both internal precipitation of mineral $AC_{(s)}$ and reaction at the zone boundaries occurs. The sharp spikes at the boundaries become Dirac delta functions in the local equilibrium limit. The numerical results using the code GEM are in excellent agreement with the semi-analytical results given by Lichtner (1991) using an entirely different method of solution.

4.2 COMPARISON OF GEM WITH ANALYTICAL SOLUTIONS FOR STEADY-STATE COUNTER-DIFFUSION

To test the cylindrical and spherical symmetry options in GEM, comparison is made with steady-state analytical solutions to pure diffusion. These are given, respectively, by:

$$C(r) = \frac{c_1 \log[r_2/r] + c_2 \log[r/r_1]}{\log[r_2/r_1]}, \quad (4-1)$$

and

$$C(r) = \frac{c_2 - c_1}{1/r_1 - 1/r_2} \left(\frac{1}{r_1} - \frac{1}{r} \right) + c_1, \quad (4-2)$$

for cylindrical and spherical geometry, respectively, where the inner concentration at $r = r_1$ has the fixed value c_1 , and the outer concentration at $r = r_2$ is fixed at c_2 . Figure 4-2 shows that there is very close agreement with GEM.

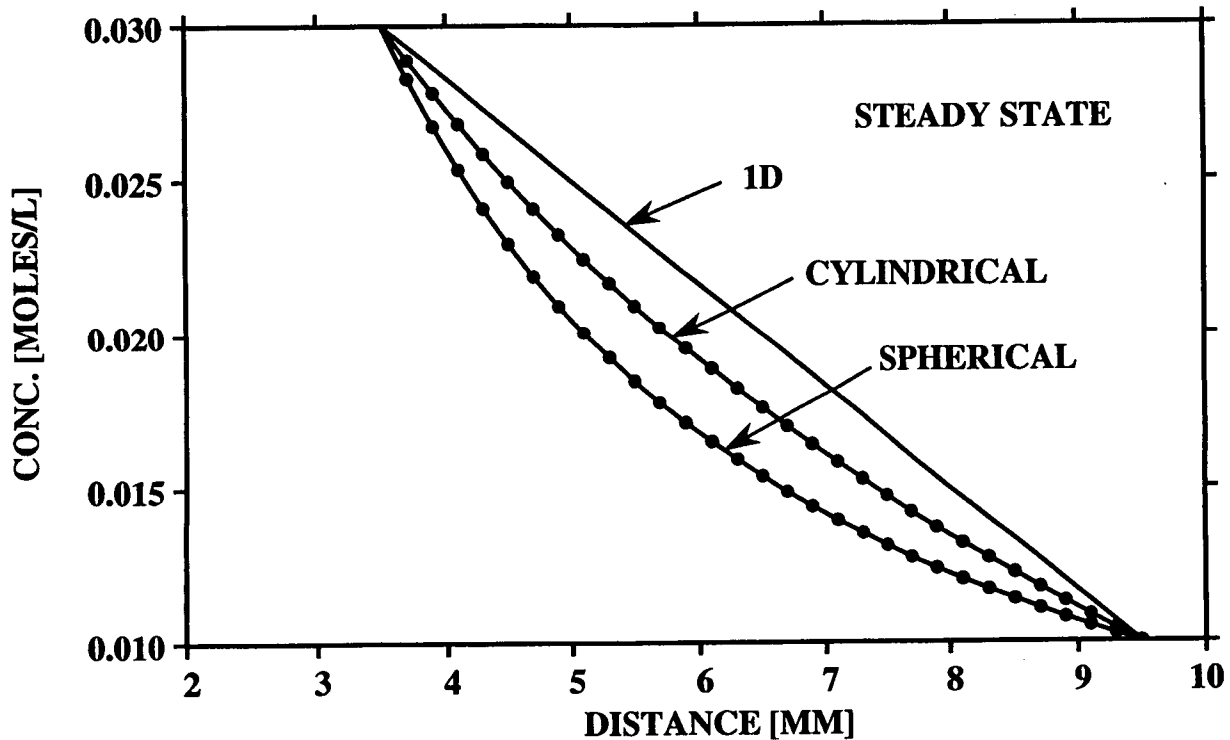


Figure 4-2. Comparison of GEM (solid curves) with analytical solutions (dots) for cylindrical and spherical geometry

4.3 ION-EXCHANGE REACTIONS

The GEM code is applied to flushing of Na^+ and K^+ from an ion-exchanger using a CaCl_2 solution. Results may be compared with Figure 10.7, page 432, of Appelo and Postma (1993), in which a similar problem is discussed. The initial fluid composition consists of a $10^{-3}M$ NaNO_3 and $2 \times 10^{-4}M$ KNO_3 solution at a pH of 5. The eluting fluid is a $6 \times 10^{-4}M$ CaCl_2 solution also at pH 5. The chloride concentration in the initial and eluting fluid is determined by charge balance. The ion-exchanger initially has equal concentrations of adsorbed Na^+ and K^+ of $0.5M$. The selectivity coefficients used in the calculation are: $k_{\text{Na}^+} = 1$, $k_{\text{K}^+} = 5$, $k_{\text{Ca}^{2+}} = 1$, and $k_{\text{H}^+} = 0.3$. The exchange capacity of the ion-exchanger is taken as $1.2M$. A fluid flow velocity of 1 my^{-1} and a diffusion coefficient of $10^{-5} \text{ cm}^2 \text{ s}^{-1}$ is used in the calculation. The resulting profile of the adsorbed ions is shown in Figure 4-3 for an elapsed time of 10 years, in qualitative agreement with Appelo and Postma (1993).

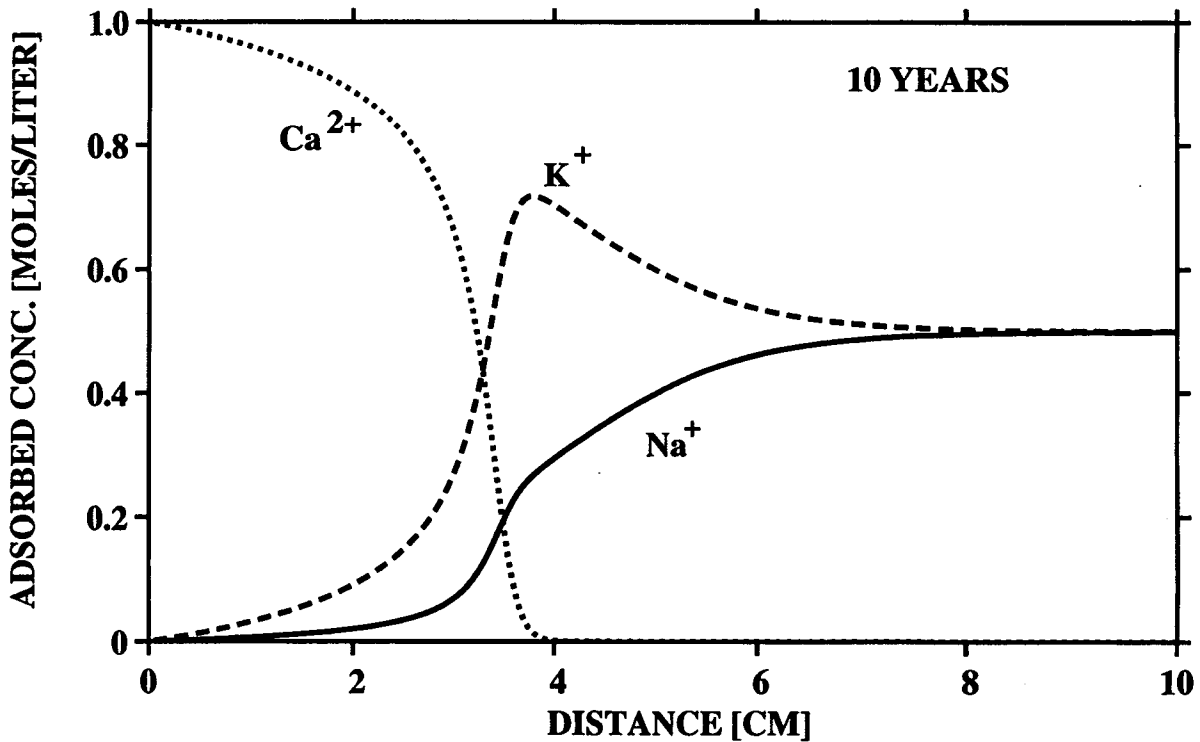


Figure 4-3. Flushing of Na^+ and K^+ by a CaCl_2 solution

5 APPLICATIONS

The time evolution of a geochemical system involving reactive transport of solutes can generally be divided into three regimes: (i) an early transient period governed by kinetic mineral reactions; (ii) an intermediate transition regime; and (iii) the asymptotic regime in which the system is in local equilibrium with the exception of narrow, compared to the total zone width, reaction fronts. In the asymptotic regime, the reaction front velocities are independent of the kinetic rate constants.

5.1 ELECTROCHEMICAL PROCESSES

As a simple illustration of electrochemical effects, consider diffusion in a NaCl-HNO₃-H₂O solution. The concentration of NaCl is assumed to be 10⁻⁴M both in the initial solution in the porous column, and in the inlet solution diffusing into the porous column. The pH is 4 in the inlet solution and 7 initially, obtained by adding different amounts of HNO₃. Because of the equal concentrations of Na⁺ and Cl⁻ in the initial and inlet solutions, in the absence of electrochemical effects there would be no change in their concentrations. However, because of the more rapid diffusion of the hydrogen ion compared to the sodium and chloride ions $D_{Na^+} = 1.4 \times 10^{-5} \text{ cm}^2 \text{ s}^{-1}$, $D_{Cl^-} = 1.2 \times 10^{-5} \text{ cm}^2 \text{ s}^{-1}$, $D_{H^+} = 9.6 \times 10^{-5} \text{ cm}^2 \text{ s}^{-1}$, $D_{OH^-} = 5.5 \times 10^{-5} \text{ cm}^2 \text{ s}^{-1}$, an electric field is established which causes the counter migration of Na⁺ and Cl⁻. This effect is illustrated in Figure 5-1. Calculations were performed with the code GEM. Solid lines refer to Na⁺ and dotted lines to Cl⁻. As a consequence of the electric field, chloride ions migrate to the left and are removed from solution, while Na⁺ ions migrate to the right increasing in concentration. With increasing concentration of NaCl, the effect becomes less pronounced because of the increased background charge of the Na⁺ and Cl⁻ ions.

5.2 COMPARISON OF GEM WITH CREVICE DIFFUSION EXPERIMENTS

The code GEM was used to compare experimental results of diffusion of an NaCl solution in a crevice in the absence of electrochemical reactions with theoretical predictions. In the experiment, the crevice was cylindrically symmetric with a gap of 10 μm. The crevice radius was 9.5 mm. The crevice was immersed in a bulk solution of known composition for a period of time so that the solution in the crevice was the same as the bulk. Then the pH of the bulk solution was altered by adding HCl to change the pH. By placing electrodes at the mouth and tip of the crevice, the change in pH within the crevice could be monitored. Different initial and bulk pH values of 2, 3, and 5 were used in the experiments.

The experimental and theoretical results are compared in Figure 5-2. The diffusion coefficients used in the calculation are given in Table 3-2. Zero flux boundary conditions were imposed at the tip and constant concentration boundary conditions at the mouth of the crevice. In Figure 5-2a, the initial pH was 2 and the inlet pH 3; in Figure 5-2b, the initial pH was 5 and the inlet pH 2; and in Figures 5-2c and 5-2d, the initial pH was 3 and the inlet pH 2. The last two figures refer to different runs of the identical experiment to test their reproducibility. The pH is plotted as a function of time for various positions within the crevice. The theoretical results correspond to the curves without symbols. In all figures, the solid curve refers to the tip of the crevice, the dashed curve to a position 3 mm from the tip, the dotted curve to a position 7 mm from the tip and the dashed-dotted curve to the mouth of the crevice. In the

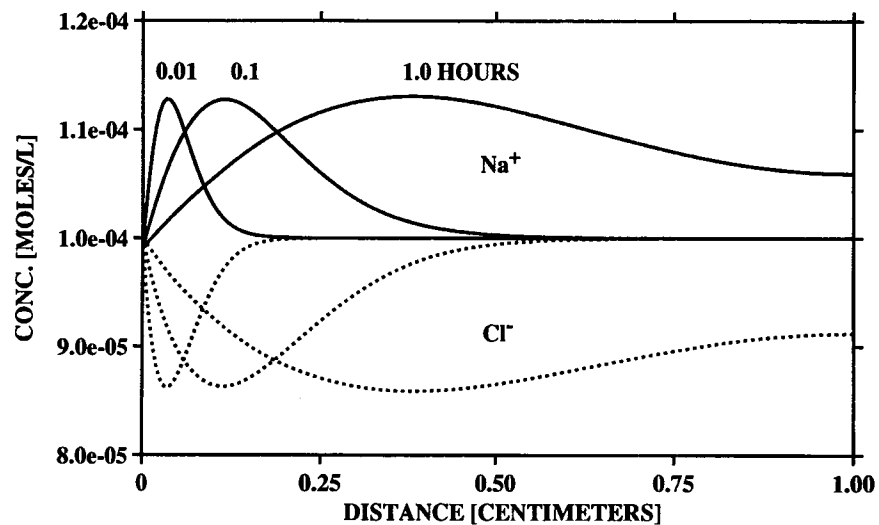


Figure 5-1. Electromigration of Na^+ and Cl^-

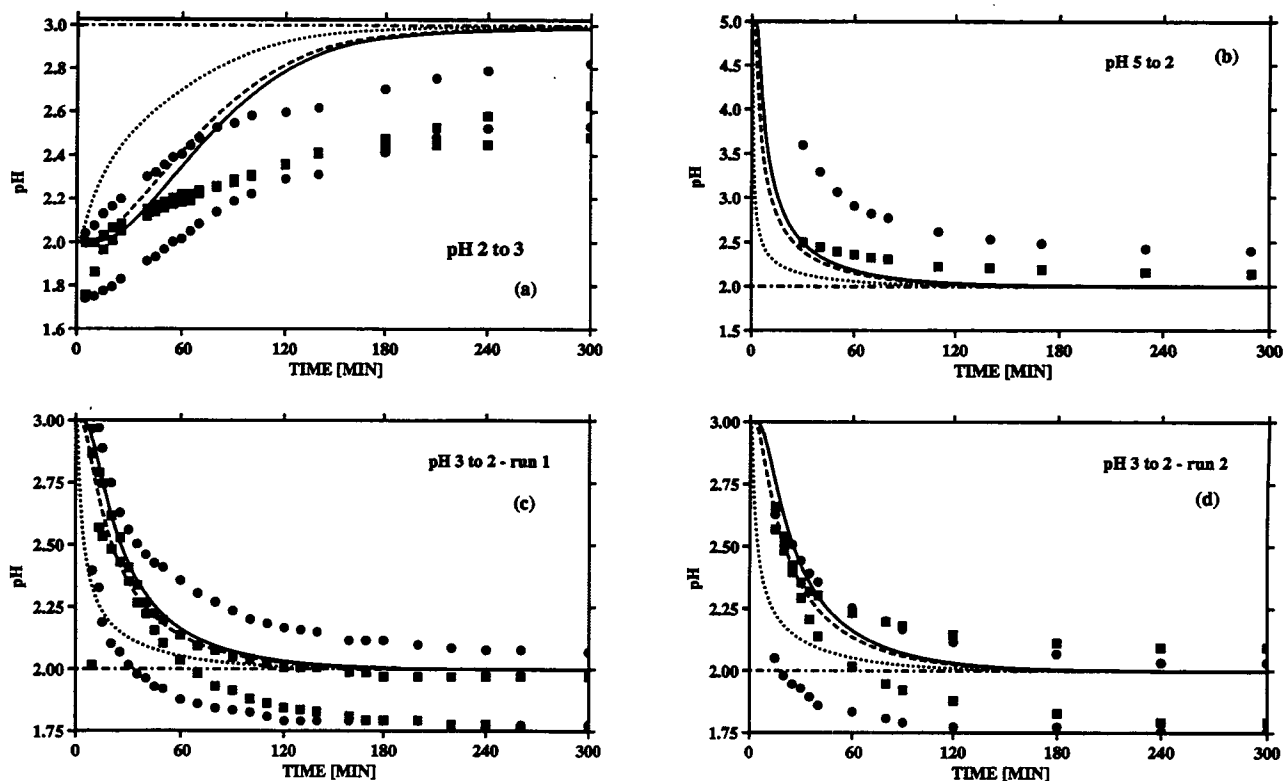


Figure 5-2. Theoretical calculations with GEM of the pH for diffusion into a crevice with species-dependent diffusion coefficients (curves) compared with experiment (symbols). (See text for further explanation.)

theoretical results, the pH at the mouth is fixed by the boundary condition imposed on the calculation and, hence, is a straight line. The experimental results are plotted as symbols, with circles referring to the tip and squares to the mouth of the crevice. Where the same symbol appears more than once at a given time, indicates measurements from two probes placed at different positions in the crevice but at the same radius.

The agreement between theory and experiment is only qualitative. The experiments tend to take somewhat longer to reach a steady-state compared to the theoretical calculations. However, there is little correlation between measurements at the mouth and tip, other than the general tendency towards a steady state. Part of the difficulty in the experiments is fixing the boundary condition at the mouth of the crevice which may account for some of the discrepancy. It should be kept in mind that the experiments are difficult to perform because of the small size of the crevice.

6 SPENT FUEL OXIDATION

An important problem in the disposal of HLW is the alteration of spent nuclear fuel under oxidizing and nonoxidizing conditions (Shoesmith and Sunder, 1992). For conditions representative of Yucca Mountain of oxidizing, partially saturated porous media and high groundwater silica concentrations, it can be expected that the alteration products of spent fuel may be replacement by the minerals soddyite and uranophane. In this section, schematic calculations are carried out with the code GEM describing the oxidation of uraninite contained in a tuffaceous host rock representative of the Peña Blanca natural analogue site. The primary mineral assemblage used in the calculation is given in Table 6-1. It is assumed in the calculations that an oxidizing fluid diffuses into a host rock with this composition and oxidizes the uraninite and pyrite-producing uranium-bearing secondary minerals and iron oxide.

The inlet fluid composition was determined by assuming the oxygen fugacity and CO₂ partial pressure to be in equilibrium with the atmosphere with values of 0.2 and 10⁻³ bars, respectively. The pH was chosen arbitrarily with the value 6. Silica was fixed by equilibrium with chalcedony, iron was determined by equilibrium with ferrihydrite, and aluminum by equilibrium with kaolinite. Sulfate concentration was taken as 10⁻⁵ molal. The

concentrations of UO₂²⁺ and Ca²⁺ were fixed by equilibrium with soddyite and uranophane. In order to obtain equilibrium with uranophane, it was necessary to modify the equilibrium constant given in the EQ3/6 database from 17.29 to 4.0, a change of 13 log units. The value of 4 for the uranophane log *K* was obtained by adjusting the log *K* until simultaneous equilibrium could be obtained with uranophane and soddyite and the oxidizing inlet fluid. The initial fluid composition was determined by equilibrium with minerals pyrite, uraninite, kaolinite, and chalcedony. The total iron and sulfur concentrations were fixed at 10⁻³ molal. The calcium concentration was fixed by charge conservation, and the chloride concentration was assumed to be the same as in the inlet fluid. A pH of 7.5 was assumed. The initial and inlet fluid compositions for the concentrations of primary species used in the calculations are presented in Table 6-2.

The results of the calculation are shown in Figures 6-1a and 6-1b for the mineral volume fractions and porosity plotted as a function of distance corresponding to an elapsed time of 1,000 years. As can be seen in the figure, uraninite is converted to soddyite and uranophane, and pyrite to ferrihydrite at an approximately common redox front. In addition, enrichment in kaolinite occurs near the inlet. These results are in qualitative agreement with field observations at the Peña Blanca natural analogue site (Percy et al., 1993). The porosity becomes strongly negative in the region where soddyite and uranophane form. This can be understood by examining the replacement reactions and the volume changes of reaction. The Eh, pH, and total uranium and iron concentration profiles are shown in Figures 6-2a and 6-2b. The aqueous uranium concentration is limited to low values as a result of the low solubilities of the uranium-bearing minerals.

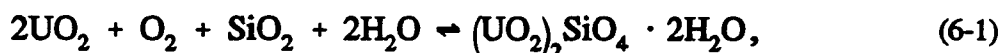
Table 6-1. Volume fractions of the primary mineral assemblage

Mineral	Volume Fraction
uraninite	0.3
pyrite	0.02
kaolinite	0.2
amorphous silica	0.45
porosity	0.03

Table 6-2. Compositions of the inlet and initial fluid. Molality units are used with the exception of pH.

Primary Species	Inlet Fluid	Initial Fluid
pH	6.0	7.5
Al ³⁺	1.8987E-12	6.0041E-17
Ca ²⁺	2.1587E-05	1.8362E-04
Fe ²⁺	2.0200E-15	8.7977E-04
SO ₄ ²⁻	9.9712E-06	8.5973E-04
SiO ₂	1.8703E-04	1.8703E-04
UO ₂ ²⁺	1.1508E-10	3.9908E-21
HCO ₃ ⁻	1.5360E-05	4.8574E-04
O _{2(aq)}	2.5277E-04	9.4364E-70
Cl ⁻	1.0900E-04	1.0900E-04

Replacement of uraninite ($\bar{V}_{uran} = 24.62 \text{ cm}^3 \text{ mole}^{-1}$) by soddyite ($\bar{V}_{sodd} = 131.27 \text{ cm}^3 \text{ mole}^{-1}$) results in the overall reaction of the form



balanced on uranium. The volume change of reaction is given by the ratio

$$\frac{\bar{V}_{sodd}}{2\bar{V}_{uran}} = 2.67, \quad (6-2)$$

and, therefore, if the replacement reaction conserves uranium in the solid phases, there must be a volume increase by the factor 2.67, which agrees with the flat portion of the soddyite volume fraction profile shown in Figure 6-1a. This results in a strong positive volume change of reaction and leads to a negative porosity in the GEM calculations as can be seen in Figure 6-1b.

Uranophane results in an even larger volume change. The reaction of uranophane is given by



with a molar volume of $224.9 \text{ cm}^3 \text{ mole}^{-1}$. The reactions must approximately conserve uranium in the calculations because of the low solubility of uranophane and soddyite.

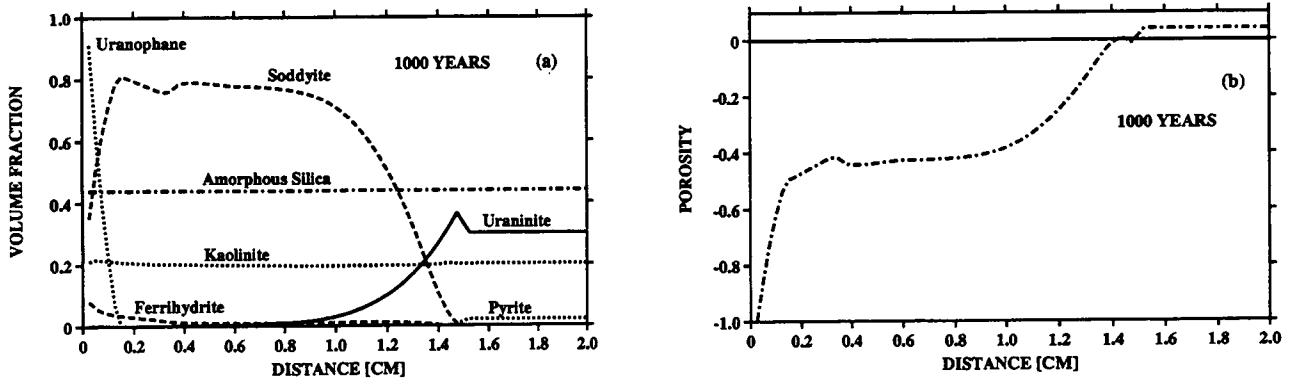


Figure 6-1. Theoretical calculations with GEM describing oxidation of uraninite in a tuffaceous host rock showing (a) volume fraction profiles, and (b) porosity for an elapsed time of 1,000 years

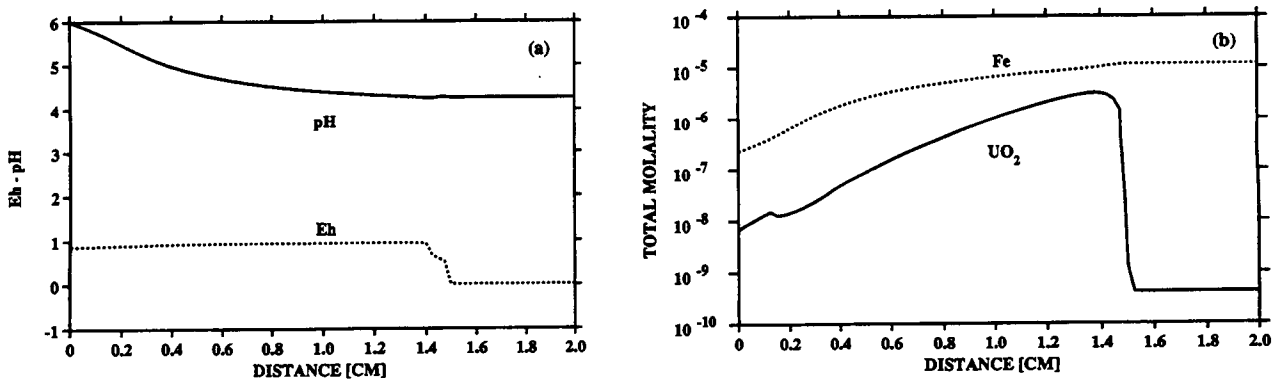
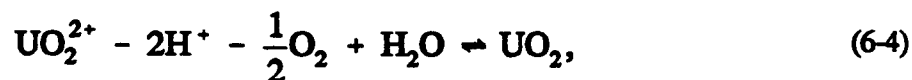
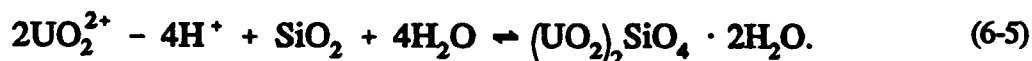


Figure 6-2. Theoretical calculations with GEM describing oxidation of uraninite in a tuffaceous host rock showing (a) Eh and pH, and (b) total uranium and iron aqueous concentrations for an elapsed time of 1,000 years

However, there are other possibilities for transforming uraninite to soddyite and uranophane. One is conservation of volume, often cited by geologists as a pseudomorphic replacement mechanism in metamorphic environments at high temperatures and pressures. To investigate the more general case, consider the individual reactions of uraninite and soddyite written in terms of a common set of primary species. The reaction for uraninite can be written as



and the reaction for soddyite as



The transport equation for dissolved uranium has the form

$$\frac{\partial \phi \Psi_{\text{UO}_2}}{\partial t} + \frac{\partial \Omega_{\text{UO}_2}}{\partial x} = -I_{\text{uran}} - 2I_{\text{sodd}} \quad (6-6)$$

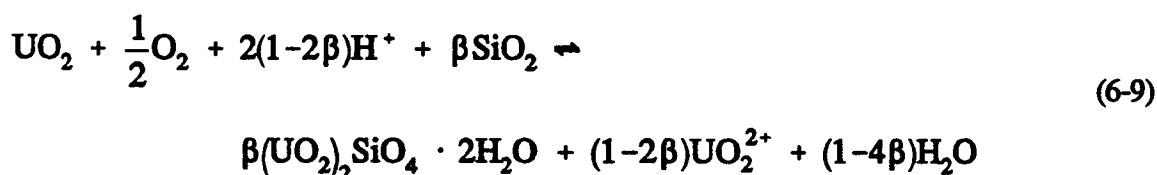
For change in volume fraction of the minerals uraninite and soddyite, the mass transfer equations are given, respectively, by

$$\frac{\partial \phi_{\text{uran}}}{\partial t} = \bar{V}_{\text{uran}} I_{\text{uran}}, \quad (6-7)$$

and

$$\frac{\partial \phi_{\text{sodd}}}{\partial t} = \bar{V}_{\text{sodd}} I_{\text{sodd}}. \quad (6-8)$$

Taking a linear combination of the reactions for uraninite and soddyite yields a single overall reaction of the general form



obtained by subtracting the reaction for soddyite multiplied by the coefficient β from the uraninite reaction. The individual reaction rates are related by the expression

$$I_{\text{sodd}} = -\beta I_{\text{uran}}. \quad (6-10)$$

In this case, the transport equation for dissolved uranium has the form

$$\frac{\partial \phi_{UO_2}}{\partial t} + \frac{\partial \Omega_{UO_2}}{\partial x} = (2\beta - 1)I_{uran}, \quad (6-11)$$

and the volume changes satisfy the relation

$$-\frac{\partial \phi_{sodd}/\partial t}{\partial \phi_{uran}/\partial t} = \beta \frac{\bar{V}_{sodd}}{\bar{V}_{uran}}. \quad (6-12)$$

If uranium is conserved in the solid phases and, hence, also the aqueous phase, then the individual reaction rates of uraninite and soddyite are related by

$$I_{sodd} = -\frac{1}{2}I_{uran}, \quad (6-13)$$

and $\beta = 1/2$, in agreement with the reaction given in Eq. (6-1). In this case, the volume changes satisfy the relation

$$-\frac{\partial \phi_{sodd}/\partial t}{\partial \phi_{uran}/\partial t} = \frac{\bar{V}_{sodd}}{2\bar{V}_{uran}} \approx 2.67, \quad (6-14)$$

as observed in Figure 6-1a. If, on the other hand, volume is to remain constant during the replacement reaction, then the volume changes must be equal and

$$-\frac{\partial \phi_{uran}/\partial t}{\partial \phi_{sodd}/\partial t} = 1. \quad (6-15)$$

In this case, the reaction rates are related by the equation

$$\bar{V}_{uran}I_{uran} + \bar{V}_{sodd}I_{sodd} = 0, \quad (6-16)$$

or

$$-\frac{I_{sodd}}{I_{uran}} = \frac{\bar{V}_{uran}}{\bar{V}_{sodd}}, \quad (6-17)$$

and

$$\beta = \frac{\bar{V}_{uran}}{\bar{V}_{sodd}} \approx 0.188. \quad (6-18)$$

To incorporate these constraints into the rate equation, the rate law can be modified to provide a specified precipitation rate far from equilibrium. In the conventional rate law, the precipitation rate grows without

bound as supersaturation increases, which is somewhat unrealistic given that eventually the rate becomes controlled by transport of solutes. However, by employing the expression

$$I_m = -k_m s_m \frac{1 - K_m Q_m}{1 + \frac{1}{f_m} K_m Q_m}, \quad (6-19)$$

where f_m is a constant, the precipitation rate can be limited to finite values as the fluid composition becomes more and more supersaturated. Far from equilibrium the rate reduces to

$$I_m = -k_m s_m, \quad Q_m \rightarrow 0, \quad (\text{dissolution}) \quad (6-20)$$

and

$$I_m = f_m k_m s_m, \quad Q_m > 1, \quad (\text{precipitation}) \quad (6-21)$$

for precipitation and dissolution. Taking the constant f_m as the ratio of molar volumes, for example:

$$f_{sodd} = \frac{\bar{V}_{uran}}{\bar{V}_{sodd}}, \quad (6-22)$$

should give a constant volume replacement reaction. However, this form of the rate results in high concentrations of uranium in solution and, hence, in highly supersaturated conditions for the minerals soddyite and uranophane as well as uraninite. Because of the extremely low solubilities of these minerals, it is unlikely that such large concentrations of uranium in solution could occur. Thus, this modification to the rate law does not provide a satisfactory resolution of the problem.

Another uranium mineral of interest that is stable under oxidizing conditions is weeksite ($K_2(UO_2)_2 Si_6O_{15} \cdot 4H_2O$) with a molar volume of $273.5 \text{ cm}^3 \text{ mole}^{-1}$. Table 6-3 summarizes the volume charge of reaction for various possibilities assuming uranium is conserved by the reaction. The column labeled volume ratio gives the ratio of the volume of the product phase to the reactant phase.

Presumably conservation of volume implies a different reaction mechanism than conservation of uranium. One possibility is that the large pressure increase that would accompany the conservation of uranium mechanism as the pore space becomes completely occupied leads to a tendency towards conservation of volume. However, the current

Table 6-3. Possible replacement reactions of uraninite and the corresponding volume change assuming uranium is conserved

Reaction	Volume Ratio
uraninite → soddyite	2.67
uraninite → uranophane	4.57
uraninite → weeksite	5.55
soddyite → uranophane	1.71
soddyite → weeksite	2.08
weeksite → uranophane	0.82

transition state based rate law used in GEM can only provide the uranium conservation mechanism. These possibilities need to be explored more fully before a definite statement can be made. The Peña Blanca natural analogue site offers a unique possibility to investigate these reactions in the field under *in situ* stress conditions.

7 STRESS CORROSION CRACKING MODELING

Although many mechanistic models of stress corrosion cracking (SCC) have been described in the literature, in which various atomic and microscopic processes involved in crack initiation and propagation are presented, few quantitative models exist. Most of the quantitative models deal only with the crack propagation stage. In the last EBSPAC Progress Report (Sridhar et al., 1993a), in which two quantitative models for crack initiation were reviewed, it was concluded that these models are not adequate for performance evaluation of container materials. Models of crack propagation, in which anodic processes are involved, were analyzed in more detail, including the film-induced cleavage, the surface mobility, and the slip-dissolution models, with the emphasis placed on the last one. It was noted that while the slip-dissolution model enjoyed some success in predicting SCC of iron-base and nickel-base alloys under conditions typical of operating nuclear power plants, particularly for stainless steel (SS) in high temperature aqueous environments, these predictions were mostly based on adjustments of the experimental results obtained in the laboratory by using field data.

As a result of the problems noted above, the approach adopted in the development of EBSPAC is based on the evaluation of the critical potential concept. The existence of a critical potential for transgranular SCC of austenitic SS in chloride-containing solutions, below which SCC does not occur, justifies an approach based on the use of this potential as a bounding parameter for evaluating the SCC resistance of a container material as discussed before (Sridhar et al., 1993a). Tsujikawa and coworkers (Tsujikawa et al., 1985, 1994; Tamaki et al., 1990) have shown that the critical potential for SCC coincides with the repassivation potential for crevice corrosion for type 316 SS and other experimental austenitic SSs in hot, dilute chloride solutions. As part of the Integrated Waste Package Experiments project, an experimental program is being conducted to evaluate the validity of this concept for type 316L SS and for alloy 825 (Sridhar et al., 1993b; 1994; Cragolino et al., 1994a). While in the case of type 316L SS, the concept seems to be applicable, the absence of SCC in alloy 825 even in highly concentrated chloride solutions, as revealed using slow strain rate tests, makes any validation difficult. Constant deflection tests are also being used to test the validity of the approach. On the other hand, an updated review of the literature did not reveal any new information on this subject.

On the basis of the limited information available and the results of the experimental work, it has been hypothesized in the example analysis of a reference container (Cragolino et al., 1994b) that SCC of austenitic Fe-Cr-Ni-Mo alloys in hot chloride solutions occurs in the range defined by the repassivation potential for localized corrosion, E_{rp} , and the nucleation potential, E_p , such that $E_{rp} < \Delta E_{SCC} < E_p$, where ΔE_{SCC} is the potential range for SCC. At potentials above E_p , pitting corrosion predominates over SCC.

The additional condition postulated for SCC to occur was that the stress intensity, K_I , at a pre-existing flaw on the container has to exceed $K_{I_{SCC}}$, the threshold stress intensity for SCC, which is a material- and environment-dependent parameter. For the purpose of the analysis, it was assumed that the value of $K_{I_{SCC}}$ is relatively high for both type 304L SS and alloy 825. A hypothetical material, with a very low $K_{I_{SCC}}$, was considered to evaluate the possibility of SCC. A value of approximately 5-10 MPa \cdot m^{1/2} can be adopted as valid in this case.

Once the conditions for SCC were established, crack initiation was assumed to occur after an induction time of about 20 years. Subcritical crack growth was then postulated to occur with a crack propagation

rate of 1.6×10^{-11} m/s, independent of stress intensity at K_I values greater than $K_{I_{SCC}}$, which is a characteristic of Stage II cracking. In principle, the approach adopted in the example problem seems to be valid for the consideration of materials with different E_{rp} and $K_{I_{SCC}}$ in a given environment. However, the description is limited and needs to be substantiated better through a combination of experimental work and modeling.

In summary, an empirical description of the SCC process was developed, based on fracture mechanics concepts coupled with the consideration of the electrochemical conditions for the initiation of cracks arising from the localized environment developed within an active crevice. Further advances in the modeling of crevice corrosion, as well as an unambiguous experimental demonstration of the relationship between the critical potential for SCC and the repassivation potential for crevice corrosion, are needed for modeling the conditions required for the occurrence of SCC in different materials. This approach needs to be developed further because, if valid, it offers an integrated view of different materials degradation processes.

8 SUMMARY

This report presents progress on computer code development within the EBSPAC program in the EBS element. During this fiscal year, enhancements to the two-phase fluid flow code VTOUGH were made resulting in a new code referred to as CTOUGH. This code has a number of improvements in I/O and computational efficiency over the original version. In addition, the computer codes TWITCH and MARIANA, developed at the CNWRA by J. Walton for describing crevice corrosion processes, were replaced with the code GEM.

The code GEM was developed to analyze crevice corrosion on metal containers and problems involving dissolution of spent fuel, as well as a diverse set of other problems involving advective and diffusive transport of solute species and their chemical reaction. The reactions included in GEM are currently homogeneous aqueous reactions, including redox reactions, dissociation of water, ion pairing and complexing reactions; heterogeneous reactions of solids with an aqueous solution including redox reactions; and ion-exchange reactions. The EQ3/6 database provides thermodynamic equilibrium constants and stoichiometric coefficients for the chemical reactions used by the GEM code.

Following a general formulation of mass conservation equations, including the effects of electromigration, in terms of a minimal set of primary species, the numerical solution algorithm used in GEM was introduced. Two benchmark problems to test parts of the code were run, one involving precipitation and dissolution of two hypothetical minerals in a three-component system for which a semi-analytical solution was available (Lichtner, 1991), and the other testing the code for transport in 2D and 3D cylindrically and spherically symmetric geometries. GEM was applied to several examples of electromigration, ion-exchange in a porous column, and diffusive transport in a 10- μm -wide crevice. In the latter example, the results were compared with experimental observations. Qualitative agreement was reasonable; however, quantitative agreement was relatively poor as a consequence of the difficulty in carrying out measurements in a tiny crevice as well as maintaining fixed concentration boundary conditions at the mouth of the crevice.

As a final example, GEM was applied to the problem of alteration of spent fuel under oxidizing conditions. Diffusion of oxidizing water into a porous medium consisting of uraninite (UO_2) and pyrite, similar to the Peña Blanca natural analogue site was considered. Two uranium-bearing alteration products, uranophane and soddyite, formed which gave qualitative agreement with the paragenesis observed at Peña Blanca (Percy et al., 1993). However, the product minerals occupied a larger volume than the original reactants resulting in a negative porosity. It was found necessary to alter the equilibrium constant for uranophane by 13 orders of magnitude from the value in the EQ3/6 database in order for uranophane to become stable. The large volume change may have significant implications for disposal of HLW above the water table, as is currently being considered at Yucca Mountain, Nevada. Because of the possibility of spalling of the alteration products due to volume expansion, it will be a very difficult task to model the alteration of spent fuel with any degree of certainty if the large positive volume change of reaction obtained in these calculations prevails. This effect will be considered further in the FY95 EBSPAC investigations.

An empirical description of the SCC process was presented, based on fracture mechanics concepts coupled with the consideration of the electrochemical conditions for the initiation of cracks arising from the localized environment developed within an active crevice. An experimental demonstration of the relationship between the critical potential for SCC and the repassivation potential for crevice corrosion

is needed for modeling the conditions required for the occurrence of SCC in different materials. This approach needs to be developed further because it can offer an integrated view of different materials degradation processes.

9 REFERENCES

- Appelo, C.A.J., and D. Postma. 1993. *Geochemistry, Groundwater, and Pollution*. Rotterdam, The Netherlands: A.A. Balkema.
- Cragolino, G., D. Dunn, and N. Sridhar. 1994a. Integrated Waste Package Experiments. *NRC High-Level Radioactive Waste Research at CNWRA. July-December 1993*. B. Sagar, ed. CNWRA 94-01S. San Antonio, TX: Center for Nuclear Waste Regulatory Analyses: 3-1-3-21.
- Cragolino, G., Sridhar, N., J.C. Walton, R. Janetzke, T. Torng, J. Wu, and P.K. Nair. 1994b. "Substantially Complete Containment"—Example Analysis of a Reference Container. CNWRA 94-003. San Antonio, TX: Center for Nuclear Waste Regulatory Analyses.
- Lasaga, A.C. 1981. Transition state theory. *Kinetics of Geochemical Processes, Reviews in Mineralogy*. A.C. Lasaga and R.J. Kirkpatrick, eds. Washington, DC: Mineralogy Society of America: 8: 135-169.
- Lichtner, P.C. 1985. Continuum model for simultaneous chemical reactions and mass transport in hydrothermal systems. *Geochimica Cosmochimica Acta* 49: 227-800.
- Lichtner, P.C. 1991. The quasi-stationary state approximation to fluid-rock reaction: Local equilibrium revisited. J. Ganguly, ed. *Advances in Physical Geochemistry* 8: 454-562.
- Lichtner, P.C. 1993. Scaling properties of kinetic mass transport equations. *American Journal of Science* 293: 257-296.
- Macdonald, D.D., and M. Urquidi-Macdonald. 1990a. Thin-layer mixed-potential model for the corrosion of high-level nuclear waste canisters. *Science* 46: 380-390.
- Macdonald, D.D. and M. Urquidi-Macdonald. 1990b. A coupled environment model for stress corrosion cracking in sensitized type 304 stainless steel in LWR environments. *Corrosion Science* 32: 51-81.
- Newman, J.S. 1991. *Electrochemical Systems*. 2nd ed. Englewood Cliffs, NJ: Prentice Hall: 560.
- Newman, J.S., and C.W. Tobias. 1962. Theoretical analysis of current distribution in porous electrodes. *Journal of the Electrochemical Society* 109: 1183-1191.
- Nitao, J.J. 1989. *VTOUGH—An Enhanced Version of the TOUGH Code for the Thermal and Hydrologic Simulation of Large-Scale Problems in Nuclear Waste Isolation*. UCID-21954. Livermore, CA: Lawrence Livermore National Laboratories.
- Oelkers, E.H., and H.C. Helgeson. 1988. Calculation of the thermodynamic and transport properties of aqueous species at high pressures and temperatures: Aqueous tracer diffusion coefficients of ions to 1000 °C and 5 kb. *Geochimica et Cosmochimica Acta* 52: 63-85.

- Pearcy, E.C., J.D. Prikryl, W.M. Murphy, and B.W. Leslie. 1993. *Uranium Mineralogy of the Nopal I Natural Analog Site, Chihuahua, Mexico*. CNWRA 93-012. San Antonio, TX: Center for Nuclear Waste Regulatory Analyses.
- Sharland, S.M. 1987. A review of the theoretical modelling of crevice and pitting corrosion. *Corrosion Science* 27: 289-323.
- Sharland, S.M. 1992. A mathematical model of the initiation of crevice corrosion in metals. *Corrosion Science* 27: 183-201.
- Sharland, S.M., C.P. Jackson, and A.J. Diver. 1989. A finite-element model of the propagation of corrosion crevices and pits. *Corrosion Science* 29: 1149-1166.
- Shoesmith, D.W., and S. Sunder. 1992. The prediction of nuclear fuel (UO₂) dissolution rates under waste disposal conditions. *Journal of Nuclear Materials* 190: 20-35.
- Sridhar, N., J.C. Walton, G.A. Cragnolino, and P.K. Nair. 1993a. *Engineered Barrier System Performance Assessment Codes (EBSPAC) Progress Report—October 1, 1992, through September 25, 1993*. CNWRA 93-021. San Antonio, TX: Center for Nuclear Waste Regulatory Analyses.
- Sridhar, N., G. Cragnolino, and D. Dunn. 1993b. Integrated Waste Package Experiments. *NRC High-Level Radioactive Waste Research at CNWRA. January-June 1993*. B. Sagar, ed. CNWRA 93-01S. San Antonio, TX: Center for Nuclear Waste Regulatory Analyses: 5-1-5-34.
- Sridhar, N., G. Cragnolino, and D. Dunn. 1994. Integrated Waste Package Experiments. *NRC High-Level Radioactive Waste Research at CNWRA. July-December 1993*. B. Sagar, ed. CNWRA 93-02S. San Antonio, TX: Center for Nuclear Waste Regulatory Analyses: 4-1-4-35.
- Tamaki, K., S. Tsujikawa, and Y. Hisamatsu. 1990. Development of a new test method for chloride stress corrosion cracking of stainless steel in dilute NaCl solutions. *Advances in Localized Corrosion*. H.S. Isaacs, U. Bertocci, J. Kruger, and S. Smialowska, eds. Houston, TX: National Association of Corrosion Engineers: 207-214.
- Tsujikawa, S., T. Shinohara, and Y. Hisamatsu. 1985. The role of crevices in comparison to pits in initiating stress corrosion cracks of type 316 stainless steel in different concentrations of MgCl₂ solutions at 80 °C. *Corrosion Cracking*. V.S. Goel, ed. Metals Park, OH: American Society for Metals: 35-42.
- Tsujikawa, S., T. Shinohara, and W. Lichang. 1994. Spot-welded specimen potentiostatically kept just above the crevice repassivation potential to evaluate stress corrosion cracking susceptibility of improved type 304 stainless steels in NaCl solutions. *Application of Accelerated Corrosion Tests to Service Life Prediction of Materials*. G.A. Cragnolino and N. Sridhar, eds. ASTM STP 1194. Philadelphia, PA: American Society for Testing and Materials: 340-354.
- Turnbull A. 1993. Review of modelling of pit propagation kinetics. *British Corrosion Journal* 28: 297-308.

- Verbrugge, M.W., D.R. Baker, and J. Newman. 1993a. Dependent-variable transformation for the treatment of diffusion, migration, and homogeneous reactions: application to a corroding pit. *Journal of Electrochemical Society* 140: 2530–2536.
- Verbrugge, M.W., D.R. Baker, and J. Newman. 1993b. Reaction in a corroding pit. *Electrochimica Acta* 38: 1649–1659.
- Walton, J.C., and S.K. Kalandros. 1992a. *TWITCH—A Model for Transient Diffusion, Electromigration, and Chemical Reaction in One Dimension, Version 1*. CNWRA 92-019. San Antonio, TX: Center for Nuclear Waste Regulatory Analyses.
- Walton, J.C., and S.K. Kalandros. 1992b. *MARIANA—A Simple Chemical Equilibrium Module, Version 1.0*. CNWRA 92-020. San Antonio, TX: Center for Nuclear Waste Regulatory Analyses.
- Wolery, T.J. 1983. *EQ3NR—A Computer Program for Geochemical Aqueous Speciation Solubility Calculations: User's Guide and Documentation*. UCRL-53414. Livermore, CA: Lawrence Livermore National Laboratories.

APPENDIX A

CTOUGH INPUT/OUTPUT MODIFICATIONS

CTOUGH INPUT/OUTPUT MODIFICATIONS

A.1 INPUT FILE SPECIFICATIONS

Element data corresponding to the keywords 'ELEM' and 'CONNE' must be read in the order of increasing row number. That is, read column-by-column with increasing depth. The elements, if not read in the above order, will result in improper calculations of coordinates of elements used in plotting. Also, this order is required for conjugate gradient methods. An example is given below to illustrate the data structure.

Example:

```
ELEME
A      1      matr1      1.e+3
A      2      matr1      1.e+3
A      3      matr3      1.e+3
.      .      .          .
A     15      matr1      1.e+4
B      1      matr1      1.e+3
B      2      matr1      1.e+3
B      3      matr3      1.e+3
B      .      .          .
B     15      matr1      1.e+4
C      1      matr1      1.e+3
C      2      matr1      1.e+3
.      .      .          .
.      .      .          .
```

```
CONNE
A      1      B      1      .....
A      2      B      2      .....
A      3      B      3      .....
.      .      .      .      .....
A     15      B     15      .....
B      1      C      1      .....
B      2      C      2      .....
.      .      .      .      .....
B     15      C     15      .....
.      .      .      .      .....
.      .      .      .      .....
A      1      A      2      .....
A      2      A      3      .....
.      .      .      .      .....
```

A.1.1 Solution Method

The program will use, by default, the Band matrix solver. For all other solvers, the solution method must be specified. It is best to specify the solution method in the input-data, even for the default method. This is done with the keyword SOLVER.

A.1.2 Evaporation Element Specification

If the cumulative evaporation is to be written for each time step for specified elements, data for such elements must be specified by a keyword 'EVAP' followed by element names, and the read sequence must be terminated by reading the last element with zeros or blank. The evaporation rate will be computed for all the elements and printed at the specified times along with the other state variables, irrespective of reading this dataset. In the absence of this keyword, no output will be written on unit dataEVP.xyp (see Section A.2). If rates are to be computed, derivatives of the cumulative evaporation with respect to time can be easily calculated, as the cumulative time is also available in this file.

Example:

```
EVAP
A   3
A   4
B   3
B   4
A   :blank line
```

Coordinate Calculations: Coordinates for each element identify the center of the block element with the origin placed at the bottom of the first column. In the above example, the element A 15 will be placed at the origin. It is assumed that all problems are 2D, and as such, the y-coordinate is designated to be zero for all elements.

A.1.3 Utility Keywords

The input data deck may contain certain utility-keywords, the use of which is optional. They are briefly outlined below.

1. Read - : comments

comments = Any comments or information the user wishes to enter including all blanks starting from column 2 through 80 inclusive. Comment cards are ignored by the simulator and used simply to clarify or introduce notes on any desired data. They can also be used for putting titles or headings on input variables, etc.

Example : ——

```
:Relative permeability of water is changed
:By a factor of 1.5
```

2. Read - IECHO

IECHO = LIST if input data images are to be printed.

= NOLIST if input data images are not to be printed.

Default value of IECHO = NOLIST

The input-data list will be written on file *.ERRS. If a partial list of input data is desired, insert a NOLIST card after which printing of the list is to be suppressed, and a LIST card from which printing is to be resumed. Repeated use of LIST and NOLIST cards will enable printing the desired sections of the total input data stream. LIST or NOLIST cards themselves will not be printed in the card images. Irrespective of IECHO options, a message giving the total number of cards read is printed prior to execution of the run.

Example:

```
|
| Data          Print card images
|
|              NOLIST
|
| Data          Suppress card images
|
|              LIST
|
| Data          Print card images
|
|              NOLIST
|
| Data          Suppress card images
|
```

3. Read - NCOL (N)

NCOL = Keyword indicating that this is the NCOL card, simply enter NCOL

N = Number of columns from column 1 to N inclusive, which will be read on subsequent data cards. This is referred to as the 'active field' of a card or line. The user may enter any comments or information beyond the active field which will be listed but not processed. The default value of N=80 is used. N must not be greater than 80. Repeated use of a NCOL card with different values of N will have the effect of widening or narrowing the width of the active field.

Example:

```
                                NCOL 60
                                |
                                |
Data                             Active field of 60 characters
                                |
                                NCOL 80
                                |
                                |
Data                             Active field of 80 characters
                                |
                                |
                                NCOL 70
                                |
Data                             Active field of 70 characters
                                |
```

4. Read - ISKIP

ISKIP = SKIP if input data is to be skipped and not processed until a NOSKIP card is encountered.

= NOSKIP if input data following this card is to be processed. This card has no effect if a SKIP card is not introduced prior to this card. It, in effect, negates the effect of a SKIP card.

If a segment or block(s) of data is not to be processed, insert a SKIP card at the beginning of such block and enter a NOSKIP card at the bottom of the block. Repeated use of SKIP and NOSKIP cards will have the effect of removing the data between SKIP and NOSKIP in the data deck during execution while preserving the entire input data intact. If a NOSKIP card is not encountered following a SKIP card, all the data from SKIP will be removed. Irrespective of LIST or NOLIST options invoked, data between SKIP and NOSKIP cards will not be echoed or listed.

Example:

```

|
|
| Data
|
| SKIP
|
| Data      Remove this data beginning
|           with SKIP until NOSKIP
|           card is encountered
|
| NOSKIP
|
| Data      Process this data beginning
|           after NOSKIP
|
|

```

A.2 OUTPUT FILES

Output is directed to several different files as tabulated below. Note that the file names are associated with the input data file name as prefix.

File Names	Unit #	Description
data.OUT	6	Output of VTOUGH including contents of unit 66 and 67 described below
data.HIS	8	Time history information for post-processing purposes
dataTMP.xyp	25	Temperature time-history at designated elements
dataTCP.xyp	30	Temperature and capillary pressure time-history at designated elements
dataSAT.xyp	35	Saturation time-history at designated elements
data.SAVE	60	Initial condition data for subsequent runs
data.BAL	61	Incremental and cumulative energy balance for each time step
data.COEF	62	Flow and accumulation coefficients: written only if specified by input data directives

File Names	Unit #	Description
data.ERRORS	63	All error messages and requested input data images
dataEVP.xyp	64	Cumulative evaporation for designated elements, for every time step
dataVELn.xyp	65	Velocity of fluids for specified time steps
dataVARn.xyp	66	Field variables including condensation rate for all elements at specified times
data.PCT	67	Capillary pressure curve depicting height versus saturation
data.MESH	3	Mesh or element file (scratch)
data.CON	4	Element connection file (scratch)
data.GEN	16	Sink/source generation file (scratch)

APPENDIX B

IMPLICIT FINITE DIFFERENCE EQUATIONS

IMPLICIT FINITE DIFFERENCE EQUATIONS

This appendix presents the finite difference equations that are programmed in the code GEM based on the equations derived in the text. Special attention is paid to the introduction of species-dependent diffusion coefficients and a numerical approach for self-consistently computing the solution current density while honoring the electroneutrality condition. A fully implicit finite difference scheme is used to solve the primary species mass transport equations.

B.1 FINITE DIFFERENCE EQUATIONS IN ONE-DIMENSIONAL, CYLINDRICAL, AND SPHERICAL GEOMETRIES

Although the code GEM applies to a 1D spatial grid, it does provide for the use of cylindrically and spherically symmetric grids. The resulting finite difference equations are reviewed briefly in this section.

B.1.1 Cylindrical Geometry

For cylindrical coordinates, the mass transport equations are

$$\frac{\partial}{\partial t}(\phi C) + \frac{1}{r} \frac{\partial}{\partial r}(rJ) = -\sum_m v_{jm} I_m, \quad (\text{B-1})$$

with the radial flux given by

$$J = -\tau \phi D \frac{\partial C}{\partial r} + vC. \quad (\text{B-2})$$

Finite difference equations are obtained by integrating over the n^{th} control volume (see Figure B-1):

$$\int_{r_{n-1/2}}^{r_{n+1/2}} \phi C 2\pi r dr = \pi (r_{n+1/2}^2 - r_{n-1/2}^2) \phi_n C_n, \quad (\text{B-3})$$

and

$$\int_{r_{n-1/2}}^{r_{n+1/2}} \frac{1}{r} \frac{\partial}{\partial r}(rJ) 2\pi r dr = 2\pi (r_{n+1/2} J_{n+1/2} - r_{n-1/2} J_{n-1/2}). \quad (\text{B-4})$$

This procedure yields the finite difference equation given by

$$\phi \frac{\Delta C_n}{\Delta t} V_n + A_{n+1/2} J_{n+1/2} - A_{n-1/2} J_{n-1/2} = -V_n \sum_m v_{jm} I_m, \quad (\text{B-5})$$

where the nodal volume is given by

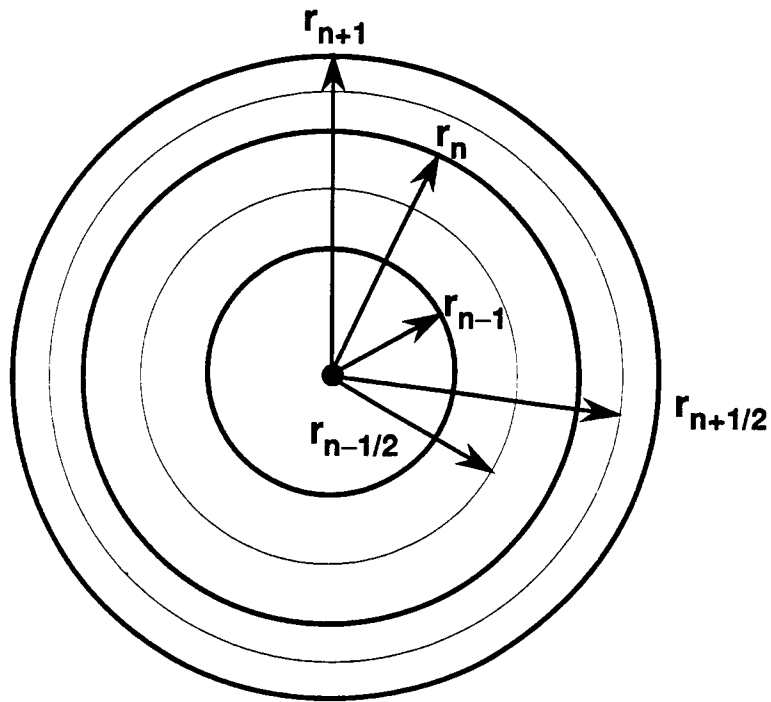


Figure B-1. Coordinates used to define cylindrically and spherically symmetric grids

$$V_n = \pi(r_{n+1/2}^2 - r_{n-1/2}^2), \quad (\text{B-6})$$

and the interface surface areas by

$$A_{n+1/2} = 2\pi r_{n+1/2} = \pi(r_{n+1} + r_n), \quad (\text{B-7})$$

$$A_{n-1/2} = 2\pi r_{n-1/2} = \pi(r_n + r_{n-1}). \quad (\text{B-8})$$

In these relations

$$r_{n+1/2} = \frac{1}{2}(r_{n+1} + r_n), \quad (\text{B-9})$$

and

$$r_{n-1/2} = \frac{1}{2}(r_n + r_{n-1}). \quad (\text{B-10})$$

The finite difference form of the diffusive flux is given by

$$J_{n+1/2} = -\phi D_{n+1/2} \frac{C_{n+1} - C_n}{r_{n+1} - r_n}, \quad (\text{B-11})$$

and

$$J_{n-1/2} = -\phi D_{n-1/2} \frac{C_n - C_{n-1}}{r_n - r_{n-1}}. \quad (\text{B-12})$$

The diffusion coefficients evaluated at the interfaces can be calculated either by the harmonic mean:

$$D_{n\pm 1/2} = \frac{D_{n\pm 1} D_n}{D_{n\pm 1} + D_n}, \quad (\text{B-13})$$

or the arithmetic mean:

$$D_{n\pm 1/2} = \frac{1}{2}(D_{n\pm 1} + D_n). \quad (\text{B-14})$$

B.1.2 Spherical Geometry

For spherical symmetry, it follows that

$$\frac{\partial}{\partial t}(\phi C) + \frac{1}{r^2} \frac{p^2}{p^2 r} (r^2 J) = -\sum_m v_{jm} I_m, \quad (\text{B-15})$$

where the radial flux has the same form as in the cylindrical case but with the coordinate r now referring to the spherical radius. Finite difference equations follow by integrating over a spherical shell as a control volume

$$\int_{r_{n-1/2}}^{r_{n+1/2}} \dots 4\pi r^2 dr. \quad (\text{B-16})$$

This gives the nodal volume

$$V_n^{\mathcal{V}} = \frac{4\pi}{3} (r_{n+1/2}^3 - r_{n-1/2}^3), \quad (\text{B-17})$$

and interface areas

$$A_{n+1/2}^{sp} = 4\pi r_{n+1/2}^2 = \pi(r_{n+1} + r_n)^2, \quad (\text{B-18})$$

$$A_{n-1/2}^{sp} = 4\pi r_{n-1/2}^2 = \pi(r_n + r_{n-1})^2. \quad (\text{B-19})$$

In terms of the solute concentration, the finite difference equations become

$$\begin{aligned} R_n = & \phi \frac{\Delta C_n}{\Delta t} V_n - \frac{\phi D A_{n+1/2}}{\Delta x_{n+1}} C_{n+1} + \phi D \left(\frac{A_{n+1/2}}{\Delta x_{n+1}} - \frac{A_{n-1/2}}{\Delta x_n} \right) C_n \\ & - \frac{\phi D A_{n-1/2}}{\Delta x_n} C_{n-1} + V_n \sum v_{jr} I_{rn} \\ & + \frac{v}{2} A_{n+1/2} C_{n+1} + \frac{v}{2} (A_{n+1/2} - A_{n-1/2}) C_n - \frac{v}{2} A_{n-1/2} C_{n-1} = 0. \end{aligned} \quad (\text{B-20})$$

writing

$$A_{n+1/2} J_{n+1/2} = -\phi D A_{n+1/2} \frac{C_{n+1} - C_n}{\Delta x_{n+1}} + \frac{v}{2} A_{n+1/2} (C_{n+1} + C_n), \quad (\text{B-21})$$

and

$$A_{n-1/2} J_{n-1/2} = -\phi D A_{n-1/2} \frac{C_n - C_{n-1}}{\Delta x_n} + \frac{v}{2} A_{n-1/2} (C_n + C_{n-1}). \quad (\text{B-22})$$

Combining terms yields

$$\begin{aligned} R_n = & \phi \frac{\Delta C_n}{\Delta t} V_n + V_n \sum v_{jr} I_{rn} \\ & + \left[\frac{v}{2} - \frac{\phi D}{\Delta x_{n+1}} \right] A_{n+1/2} C_{n+1} \\ & + \left[\frac{v}{2} (A_{n+1/2} - A_{n-1/2}) + \phi D \left(\frac{A_{n+1/2}}{\Delta x_{n+1}} + \frac{A_{n-1/2}}{\Delta x_n} \right) \right] C_n \\ & - \left[\frac{v}{2} + \frac{\phi D}{\Delta x_n} \right] A_{n-1/2} C_{n-1} = 0. \end{aligned} \quad (\text{B-23})$$

By comparison, in one dimension

$$V_n^{1D} = \delta x_n = x_{n+1/2} - x_{n-1/2} = \frac{1}{2} (x_{n+1} - x_{n-1}) = \frac{1}{2} (\Delta x_{n+1} + \Delta x_n), \quad (\text{B-24})$$

and

$$A_{n+1/2}^{1D} = A_{n-1/2}^{1D} = 1, \quad (\text{B-25})$$

where

$$\Delta x_n = x_n - x_{n-1}. \quad (\text{B-26})$$

The finite difference equations simplify to

$$\phi \frac{\Delta C}{\Delta t} \delta x_n + J_{n+1/2} - J_{n-1/2} = -\delta x_n \sum_m v_{jm} I_{mn}. \quad (\text{B-27})$$

B.2 Zero-Flux Boundary Conditions

Zero-flux boundary conditions for diffusive transport at the inlet or outlet of the porous column are implemented using a fictitious node point outside the boundary. For the N^{th} node point, this leads to the condition:

$$\Psi_{j,N+1} = \Psi_{jN}. \quad (\text{B-28})$$

The residual flux term then becomes

$$R_{jN} = (\beta_N + \alpha_N) \Psi_{jN} + \gamma_N \Psi_{j,N-1}. \quad (\text{B-29})$$

For zero flux at the first node point, assumed to coincide with the inlet, the condition is

$$\Psi_{j0} = \Psi_{j1}. \quad (\text{B-30})$$

In this case, the residual flux term becomes

$$R_{j1} = \beta_1 \Psi_{j2} + (\alpha_1 + \gamma_1) \Psi_{j1}. \quad (\text{B-31})$$

B.3 Species-Dependent Diffusion Coefficients

B.3.1 Residuals

Finite difference equations for species-dependent diffusion coefficients and constant porosity are described next. The general form of the residuals is given by

$$R_{jn} = R_{jn}^0 + R_{jn}^{\Gamma} + R_{jn}^e, \quad (\text{B-32})$$

where

$$\begin{aligned}
R_{jn}^0 &= \phi \frac{\Psi_{jn}^{t+\Delta t} - \Psi_{jn}^t}{\Delta t} V_n + V_n \sum_r v_{jr} I_{rn} + V_n \sum_k v_{jk} I_{kn}^{corr} \\
&+ A_{n+1/2} \Delta_{jn,+1/2} - A_{n-1/2} \Delta_{j,n-1/2}, \\
&+ \phi \frac{\Psi_{jn}^{t+\Delta t} - \Psi_{jn}^t}{V_n} + \sum_r v_{jn} I_{rn} V_n \\
&- \phi \frac{A_{n+1/2} \Psi_{j,n+1}^D}{\Delta x_{n+1}} + \phi \left(\frac{A_{n+1/2}}{\Delta x_{n+1}} + \frac{A_{n-1/2}}{\Delta x_n} \right) \Psi_{jn}^D - \phi \frac{A_{n-1/2}}{\Delta x_n} \Psi_{j,n-1}^D \\
&+ \frac{v}{2} [A_{n+1/2} \Psi_{j,n+1} + (A_{n+1/2} - A_{n-1/2}) \Psi_{jn} - A_{n-1/2} \Psi_{j,n-1}],
\end{aligned} \tag{B-33}$$

$$\begin{aligned}
R_{jn}^\Gamma &= \phi(\omega)_{n+1/2} A_{n+1/2} \sum_k z_k \frac{\Psi_{k,n+1}^D - \Psi_{kn}^D}{\Delta x_{n+1}} \\
&- \phi(\omega)_{n-1/2} A_{n-1/2} \sum_k z_k \frac{\Psi_{kn}^D - \Psi_{k,n-1}^D}{\Delta x_n},
\end{aligned} \tag{B-34}$$

and

$$R_{jn}^e = \frac{1}{F} \{ (\omega)_{n+1/2} A_{n+1/2} i_{n+1/2} - (\omega)_{n-1/2} A_{n-1/2} i_{n-1/2} \}. \tag{B-35}$$

With some rearrangement, the residuals can be expressed in the form

$$\begin{aligned}
R_{jn}^0 &= \phi \frac{\Psi_{jn}^{t+\Delta t} - \Psi_{jn}^t}{\Delta t} V_n + \sum_r v_{jr} I_{rn} V_n \\
&+ \beta_n \Psi_{j,n+1} + \alpha_n \Psi_{jn} + \gamma_n \Psi_{j,n-1} \\
&+ \beta_n^D \Psi_{j,n+1}^D + \alpha_n^D \Psi_{jn}^D + \gamma_n^D \Psi_{j,n-1}^D,
\end{aligned} \tag{B-36}$$

and

$$R_{jn}^{\Gamma} = \beta_{jn}^{\Gamma} \sum_k z_k \Psi_{k,n+1}^D + \alpha_{jn}^{\Gamma} \sum_k z_k \Psi_{kn}^D + \gamma_{jn}^{\Gamma} \sum_k z_k \Psi_{k,n-1}^D. \quad (\text{B-37})$$

The various coefficients appearing in these expressions are given by

$$\alpha_n = \frac{\nu}{2} (A_{n+1/2} - A_{n-1/2}), \quad (\text{B-38})$$

$$\beta_n = \frac{\nu}{2} A_{n+1/2}, \quad (\text{B-39})$$

$$\gamma_n = -\frac{\nu}{2} A_{n-1/2}, \quad (\text{B-40})$$

$$\alpha_n^D = \phi \left(\frac{A_{n+1/2}}{\Delta x_{n+1}} + \frac{A_{n-1/2}}{\Delta x_n} \right), \quad (\text{B-41})$$

$$\beta_n^D = -\phi \frac{A_{n+1/2}}{\Delta x_{n+1}}, \quad (\text{B-42})$$

$$\gamma_n^D = -\phi \frac{A_{n-1/2}}{\Delta x_n}, \quad (\text{B-43})$$

$$\alpha_{jn}^{\Gamma} = - \left(\frac{\phi A_{n+1/2}(\omega_j)_{n+1/2}}{\Delta x_{n+1}} + \frac{\phi A_{n-1/2}(\omega_j)_{n-1/2}}{\Delta x_n} \right), \quad (\text{B-44})$$

$$\beta_{jn}^{\Gamma} = \frac{\phi A_{n+1/2}(\omega_j)_{n+1/2}}{\Delta x_{n+1}}, \quad (\text{B-45})$$

$$\gamma_{jn}^{\Gamma} = \frac{\phi A_{n-1/2}(\omega_j)_{n-1/2}}{\Delta x_n}. \quad (\text{B-46})$$

The coefficients are related by the equations

$$\alpha_n = \beta_n + \gamma_n, \quad (\text{B-47})$$

$$\alpha_n^D = -(\beta_n^D + \gamma_n^D), \quad (\text{B-48})$$

and

$$\alpha_{jn}^\Gamma = -(\beta_{jn}^\Gamma + \gamma_{jn}^\Gamma). \quad (\text{B-49})$$

The quantities $\Omega_{j,n+1/2}$ evaluated at the node interfaces have the possible forms

$$\omega_{j,n+1/2} = \frac{1}{2}(\omega_{j,n+1} + \omega_{jn}) \quad (\text{B-50})$$

and

$$\omega_{j,n+1/2} = \frac{2\omega_{j,n+1}\omega_{jn}}{\omega_{j,n+1} + \omega_{jn}}, \quad (\text{B-51})$$

corresponding to arithmetic and geometric means.

B.3.2 Electroneutrality: Self-Consistent Calculation of Solution Current Density

The condition for electroneutrality yields the relation

$$F \sum_j z_j R_{jn} = A_{n+1/2} i_{n+1/2} - A_{n-1/2} i_{n-1/2} = V_n \sum_k i_{kn} = 0, \quad (\text{B-52})$$

where

$$i_k = -\frac{Fl_g}{2} \sum_{jk} z_j \nu_{jk} J_k^{corr} = -\frac{Fl_g}{2} \sum_k n_k J_k^{corr}. \quad (\text{B-53})$$

This result must be consistent with the derivative form

$$\frac{\partial i}{\partial r} = \sum_k i_k, \quad (\text{B-54})$$

which follows directly from the mass conservation equations and electroneutrality. The current should be calculated at the node interfaces from the recursion relation

$$\begin{aligned}
i_{n+1/2} &= \frac{A_{n-1/2}}{A_{n+1/2}} i_{n-1/2} - \frac{V_n}{A_{n+1/2}} \sum_k i_{kn}, \\
&= \frac{A_{n-1/2}}{A_{n+1/2}} i_{n-1/2} + \frac{V_n}{A_{n+1/2}} \frac{Fl_g}{2} \sum_k n_k I_{kn}^{corr},
\end{aligned}
\tag{B-55}$$

which then conserves charge identically. Alternatively, depending on the boundary conditions, it may be advantageous to use the form

$$\begin{aligned}
i_{n-1/2} &= \frac{A_{n+1/2}}{A_{n-1/2}} i_{n+1/2} + \frac{V_n}{A_{n-1/2}} \sum_k i_{kn}, \\
&= \frac{A_{n+1/2}}{A_{n-1/2}} i_{n+1/2} - \frac{V_n}{A_{n-1/2}} \frac{Fl_g}{2} \sum_k n_k I_{kn}^{corr}.
\end{aligned}
\tag{B-56}$$

B.3.3 Jacobian Matrix

The Jacobian matrix is defined by

$$\begin{aligned}
J_{jn,lm} &= \frac{\partial R_{jn}}{\partial \ln C_{lm}}, \\
&= \frac{\partial R_{jn}^0}{\partial \ln C_{lm}} + \frac{\partial R_{jn}^\Gamma}{\partial \ln C_{lm}} + \frac{\partial R_{jn}^e}{\partial \ln C_{lm}}.
\end{aligned}
\tag{B-57}$$

The first two terms are given by:

$$\begin{aligned}
\frac{\partial R_{jn}^0}{\partial \ln C_{lm}} &= \frac{\phi}{\Delta t} \frac{\partial \Psi_{jn}}{\partial \ln C_{lm}} V_n \delta_{mn} + \sum_r v_{jr} \frac{\partial I_{rn}}{\partial \ln C_{lm}} V_n \\
&+ \beta_n \delta_{m,n+1} \frac{\partial \Psi_{j,n+1}}{\partial \ln C_{lm}} + \alpha_n \delta_{mn} \frac{\partial \Psi_{jn}}{\partial \ln C_{lm}} + \gamma_n \delta_{m,n-1} \frac{\partial \Psi_{j,n-1}}{\partial \ln C_{lm}} \\
&+ \beta_n^D \delta_{m,n+1} \frac{\partial \Psi_{j,n+1}^D}{\partial \ln C_{lm}} + \alpha_n^D \delta_{mn} \frac{\partial \Psi_{jn}^D}{\partial \ln C_{lm}} + \gamma_n^D \delta_{m,n-1} \frac{\partial \Psi_{j,n-1}^D}{\partial \ln C_{lm}},
\end{aligned}
\tag{B-58}$$

and

$$\begin{aligned} \frac{\partial R_{jn}^\Gamma}{\partial \ln C_{lm}} &= \beta_{jn}^\Gamma \sum_k z_k \frac{\partial \Psi_{k,n+1}^D}{\partial \ln C_{lm}} + \alpha_{jn}^\Gamma \sum_k z_k \frac{\partial \Psi_{kn}^D}{\partial \ln C_{lm}} + \gamma_{jn}^\Gamma \sum_k z_k \frac{\partial \Psi_{k,n-1}^D}{\partial \ln C_{lm}} \\ &+ \frac{\partial \beta_{jn}^\Gamma}{\partial \ln C_{lm}} \sum_k z_k \Psi_{k,n+1}^D + \frac{\partial \alpha_{jn}^\Gamma}{\partial \ln C_{lm}} \sum_k z_k \Psi_{kn}^D + \frac{\partial \gamma_{jn}^\Gamma}{\partial \ln C_{lm}} \sum_k z_k \Psi_{k,n-1}^D. \end{aligned} \quad (\text{B-59})$$

The Jacobian matrix corresponding to the current density term has the form

$$\begin{aligned} J_{jn,lm}^e &= \frac{\partial R_{jn}^e}{\partial \ln C_{lm}}, \\ &= \frac{1}{F} \left(A_{n+1/2} \frac{\partial \omega_{j,n+1/2} i_{n+1/2}}{\partial \ln C_{lm}} - A_{n-1/2} \frac{\partial \omega_{j,n-1/2} i_{n-1/2}}{\partial \ln C_{lm}} \right). \end{aligned} \quad (\text{B-60})$$

Non-zero terms are:

$$\frac{\partial R_{jn}^e}{\partial \ln C_{l,n+1}} = \frac{1}{2F} A_{n+1/2} \frac{\partial \omega_{j,n+1} i_{n+1}}{\partial \ln C_{l,n+1}}, \quad (\text{B-61})$$

$$\frac{\partial R_{jn}^e}{\partial \ln C_{lm}} = \frac{1}{2F} [A_{n+1/2} i_{n+1} - A_{n-1/2} i_n] \frac{\partial \omega_{jn}}{\partial \ln C_{lm}}, \quad (\text{B-62})$$

$$\frac{\partial R_{jn}^e}{\partial \ln C_{l,n-1}} = \frac{1}{2F} A_{n-1/2} \frac{\partial \omega_{j,n-1} i_n}{\partial \ln C_{l,n-1}}. \quad (\text{B-63})$$

To compute the Jacobian analytically, the following partial derivatives are required:

$$\frac{\partial \Gamma_j}{\partial \ln C_l} = \frac{\Gamma_j}{\Psi_j^\epsilon} \left\{ \frac{\partial \Psi_j^\epsilon}{\partial \ln C_l} - \omega_j \sum_k z_k \frac{\partial \Psi_k^\epsilon}{\partial \ln C_l} \right\}, \quad (\text{B-64})$$

and

$$\frac{\partial R_{jn}^\Gamma}{\partial \ln C_{l,n+1}} = \beta_{jn}^\Gamma \frac{\partial f_{n+1}}{\partial \ln C_{l,n+1}} + \frac{\partial \beta_{jn}^\Gamma}{\partial \ln C_{l,n+1}} f_{n+1} + \frac{\partial \alpha_{jn}^\Gamma}{\partial \ln C_{l,n+1}} f_n, \quad (\text{B-65})$$

$$\frac{\partial R_{jn}^\Gamma}{\partial \ln C_{ln}} = \alpha_{jn}^\Gamma \frac{\partial f_n}{\partial \ln C_{ln}} + \frac{\partial \beta_{jn}^\Gamma}{\partial \ln C_{ln}} f_{n+1} + \frac{\partial \alpha_{jn}^\Gamma}{\partial \ln C_{ln}} f_n + \frac{\partial \gamma_{jn}^\Gamma}{\partial \ln C_{ln}} f_{n-1}, \quad (\text{B-66})$$

$$\frac{\partial R_{jn}^\Gamma}{\partial \ln C_{l,n-1}} = \gamma_{jn}^\Gamma \frac{\partial f_{n-1}}{\partial \ln C_{l,n-1}} + \frac{\partial \alpha_{jn}^\Gamma}{\partial \ln C_{l,n-1}} f_n + \frac{\partial \gamma_{jn}^\Gamma}{\partial \ln C_{l,n-1}} f_{n-1}, \quad (\text{B-67})$$

where

$$f_n = \sum_l z_l \Psi_{ln}^D. \quad (\text{B-68})$$

For the special case of arithmetic mean values of Γ_j at node interfaces, the derivatives of the coefficient matrices are given by

$$\frac{\partial \alpha_{jn}^\Gamma}{\partial \ln C_{l,n+1}} = -\frac{\phi A_{n+1/2}}{2 \Delta x_{n+1}} \frac{\partial \omega_{j,n+1}}{\partial \ln C_{l,n+1}}, \quad (\text{B-69})$$

$$\frac{\partial \alpha_{jn}^\Gamma}{\partial \ln C_{ln}} = -\frac{\phi}{2} \left(\frac{A_{n+1/2}}{\Delta x_{n+1}} + \frac{A_{n-1/2}}{\Delta x_n} \right) \frac{\partial \omega_{jn}}{\partial \ln C_{ln}}, \quad (\text{B-70})$$

$$\frac{\partial \alpha_{jn}^\Gamma}{\partial \ln C_{l,n-1}} = -\frac{\phi A_{n-1/2}}{2 \Delta x_n} \frac{\partial \omega_{j,n-1}}{\partial \ln C_{l,n-1}}, \quad (\text{B-71})$$

$$\frac{\partial \beta_{jn}^\Gamma}{\partial \ln C_{l,n+1}} = \frac{\phi A_{n+1/2}}{2 \Delta x_{n+1}} \frac{\partial \omega_{j,n+1}}{\partial \ln C_{l,n+1}}, \quad (\text{B-72})$$

$$\frac{\partial \beta_{jn}^\Gamma}{\partial \ln C_{ln}} = \frac{\phi A_{n+1/2}}{2 \Delta x_{n+1}} \frac{\partial \omega_{jn}}{\partial \ln C_{ln}}, \quad (\text{B-73})$$

$$\frac{\partial \gamma_{jn}^\Gamma}{\partial \ln C_{ln}} = \frac{\phi A_{n-1/2}}{2 \Delta x_n} \frac{\partial \omega_{jn}}{\partial \ln C_{ln}}, \quad (\text{B-74})$$

$$\frac{\partial \gamma_{jn}^{\Gamma}}{\partial \ln C_{l,n-1}} = \frac{\phi A_{n-1/2}}{2 \Delta x_n} \frac{\partial \omega_{j,n-1}}{\partial \ln C_{l,n-1}}. \quad (\text{B-75})$$

With these results, the Jacobian matrix becomes

$$\frac{\partial R_{jn}^{\Gamma}}{\partial \ln C_{l,n+1}} = \beta_{jn}^{\Gamma} \frac{\partial f_{n+1}}{\partial \ln C_{l,n+1}} + \frac{\phi A_{n+1/2}}{2 \Delta x_{n+1}} (f_{n+1} - f_n) \frac{\partial \omega_{j,n+1}}{\partial \ln C_{l,n+1}}, \quad (\text{B-76})$$

$$\frac{\partial R_{jn}^{\Gamma}}{\partial \ln C_{ln}} = \alpha_{jn}^{\Gamma} \frac{\partial f_n}{\partial \ln C_{ln}} + \frac{\phi}{2} \left[\frac{A_{n+1/2}}{\Delta x_{n+1}} (f_{n+1} - f_n) - \frac{A_{n-1/2}}{\Delta x_n} (f_n - f_{n-1}) \right] \frac{\partial \omega_{jn}}{\partial \ln C_{ln}}, \quad (\text{B-77})$$

$$\frac{\partial R_{jn}^{\Gamma}}{\partial \ln C_{l,n-1}} = \gamma_{jn}^{\Gamma} \frac{\partial f_{n-1}}{\partial \ln C_{l,n-1}} - \frac{\phi A_{n-1/2}}{2 \Delta x_n} (f_n - f_{n-1}) \frac{\partial \omega_{j,n-1}}{\partial \ln C_{l,n-1}}. \quad (\text{B-78})$$